From the Klinik für Urologie und Kinderurologie

Director: Prof. Dr. Klaus-Peter Jünemann

at the University Medical Center Schleswig-Holstein, Campus Kiel

at Kiel University

Development of a model for the two major types of prostate carcinomas that enables the detection and study of potential markers for predicting metastasis into lymph nodes

Dissertation

to acquire the doctoral degree (Dr. med.)

at the Faculty of Medicine

at Kiel University

presented by

Ioannis Papasotiriou

from Munich

Kiel 2022

1st Reviewer: Prof. Dr. Klaus-Peter Jünemann

2nd Reviewer: PD Dr. Ulf Lützen

Date of oral examination: 16th of December 2022

Approved for printing, Kiel,

Signed:

Prof. Dr. Daniar Osmonov

(Chairperson of the Examination Committee)

Contents

Introduction

Prostate cancer is the most frequent type of cancer among men worldwide. A prostate carcinoma can be hormone-refractory or hormone-sensitive. Depending on the type, a different treatment management is pursued. Hormone-refractory prostate carcinomas exhibit a different protein profile on the surface and different abilities of migration and interaction with organs and tissues than hormone-sensitive migrating and metastasizing prostate carcinoma.

A typical prostate in adult men is 3 centimeters long and weighs 20 grams. It is part of the reproductive system and helps to produce and store seminal fluid. The prostate contains many small glands. In prostate cancer, the cells of these glands mutate into cancer cells. Male hormones, known as androgens, are essential for the proper working of the prostate glands. A prostate cancer is classified as adenocarcinoma or glandular cancer if normal gland cells mutate into cancer cells. An adenocarcinoma is most common in the peripheral zone of the prostate gland. At the beginning, small clumps of cancer cells remain confined to normal prostate glands, a condition known as 'carcinoma in situ' or 'prostate intraepithelial neoplasia'. Over time, cancer cells multiply and spread to the surrounding tissue forming a tumor. Finally, the tumor may grow large and may be able to invade nearby organs. Also, it may develop the ability to invade and travel in the blood stream and lymphatic system. This invasion is called 'metastasis'. Prostate cancer most commonly metastasizes to the bones and lymph nodes and after local progression may invade the rectum, bladder, and lower ureters. Metastasis to the bones is thought to be venous, as the prostate venous plexus, draining the prostate, connects with the vertebral veins (Mustafa et al. 2016).

The prostate cancer metastasis to bones is thought of as an osteoblastic process, but there is also abnormal osteoclastic activity. Osteoclasts are able to adhere to the surface of bone through integrin αvβ3, which is an integrin upregulated in prostate adenocarcinomas, but not found in normal prostate tissue. When osteoclasts adhere to bones, they demineralize the bone matrix and destroy matricellular proteins. They create a pit on the surface of bones and secret enzymes that signal a degradation of underlying bone. That condition is counterbalanced by osteoblasts which derive from mesenchymal stem cells, synthesize bone matrix collagenase, and thus rebuild bone. This harmony is dysregulated in skeletal metastases, a process which starts before tumor cells proliferate in bone (Autio and Morris 2013).

It has been demonstrated that lymph node metastasis might be associated with tumor-associated lymphangiogenesis. Growth factors secreted by tumor contribute to the creation of new lymphatic vessels from a precursor. VEGF family molecules are the most well-studied and well-known to be involved in lymphangiogenesis. There are controversies as to the relationship between lymphangiogenesis and prostate cancer lymph node metastasis. However, scientists agree that one possible mechanism is the increased invasion of tumor cells into the peritumoral lymphatics and/or the increase of peritumoral lymphatic vessel density (Datta et al. 2010).

The aim of the present study is to analyze the different prostate carcinoma cell lines, grown in a model environment resembling the environment of bones or lymph nodes, in order to detect biomarkers that indicate whether metastasis will take place through bones or lymph nodes. The prostate metastatic cancer cell lines were explanted from a bone metastasis and cultured in model culture environment. Specifically, a cell 3D culture was developed with an extracellular matrix (ECM) deriving from a product of Tissue Engineered Osteoblast (TEB) based on cell sheet techniques and the prostate cancer cell lines as seeded to this culture (co-cultured). The lymph nodes were developed similarly, namely on a co-cultivation model between endothelial cell lines and the relevant prostate cancer cell lines. The above experiments were repeated, with relevant depletion or inhibition of the relevant markers or membrane proteins, in order to prove the value of the concept, i.e. to study particular proteins and their role in colonization and metastases formation according to a specific metastatic pattern. Proteins that were found to be overexpressed were knocked down by using siRNA techniques. The experiments of culturing and cell interaction were repeated in order to validate, in an *in vitro* cell culturing model, the role of the related proteins in the metastases process and their interaction with specific types of cells.

To sum up, this experimental study aims to answer the question whether there are specific genes whose expression might be essential for lymph node metastasis, which would mean that a surgical removal of lymph nodes may be beneficial for the patient.

Materials & Methods

Cell Lines

We selected two types of human prostate carcinoma cancer cell lines: one group of hormone-sensitive cell lines and one group of hormone-refractory cell lines that had developed bone metastases.

The first group consisted of three cell lines: **LNCap**, **VCaP** and **MDA-PCa-2b**. LNCap clone FGC (89110211, ECACC) derived from a metastasis at the left supraclavicular lymph node of a 50-year-old patient with a confirmed diagnosis of metastatic prostate carcinoma. It was an adherent cell line cultured in RPMI 1640 culture medium (R0883, Sigma) with 2 mM Glutamine (G5792-1KG, Sigma), 1.0 mM sodium pyruvate (S8636, Sigma), 10% Fetal Bovine Serum (FBS) (F9665, Sigma) and 1% hydroxyethyl piperazineethanesulfonic acid (HEPES) (H0887-100ML, Sigma) (Horoszewicz et al. 1983). The second cell line was the VCaP (06020201, ECACC) cell line, established from prostate cancer tissue harvested from a metastatic lesion to a lumbar vertebral body of a patient with hormone-refractory prostate cancer. The cells were reported to express large quantities of prostate specific antigen (PSA). This cell line also expressed prostatic acid phosphatase (PAP) cytokeratin-18 and the androgen receptor and was androgen-sensitive *in vitro* and *in vivo*. This cell line came from a cell-based model system of human prostate cancer. It was an adherent cell line cultured in DMEM (D5546, Sigma): Ham's F12 (N4888, Sigma) (1:1) culture mediums with 2 mM Glutamine and 10% Fetal Bovine Serum (FBS) (Korenchuk et al. 2001). The third cell line was the MDA-PCa-2b (CRL-2422™, ATCC®) established from a bone metastasis of a 63-year-old black male with androgen-independent adenocarcinoma of the prostate. The cell line expressed prostate specific antigen (PSA) and androgen receptor, grew *in vitro* and *in vivo* and was androgen-sensitive. It was an adherent cell line cultured in F-12K Medium with 20% Fetal Bovine Serum (FBS), 25 ng/ml cholera toxin (C8052, Sigma), 10 ng/ml mouse Epidermal Growth Factor (354010, Corning), 0.005 mM phosphoethanolamine (P0503, Sigma), 100 pg/ml hydrocortisone (H0135, Sigma), 45 nM sodium selenite (9133, Sigma) and 0.005 mg/ml human recombinant insulin (12585-014, Life Technologies) (Navone et al. 1997).

The hormone-insensitive group also consisted of three cell lines: **PC-3**, **DU 145** and **SerBob**. PC-3 (90112714, ECACC) was established from a grade 4 prostatic adenocarcinoma from a 62-

year-old male Caucasian. It exhibited low acid phosphatase and testosterone-5-alpha reductase activity. It was an adherent cell line cultured in DMEM culture medium with 2 mM Glutamine and 10% Fetal Bovine Serum (FBS) (Ware et al. 1982). DU 145 (HTB-81™, ATCC®) was established from a prostate carcinoma derived from a metastatic site in the brain of a 69-year-old male Caucasian. It was an adherent cell line cultured in EMEM culture medium (30-2003, ATCC) with 2 mM Glutamine and 10% Fetal Bovine Serum (FBS) (Stone et al. 1978). SerBob (10021101, ECACC) was the first spontaneously immortalized prostate cancer cell line to be established from a transrectal needle biopsy (TRBP) of a patient with castration-resistant prostate cancer (CRPC). SerBob grew as a monolayer culture with limited differentiation. It was an adherent cell line cultured in Keratinocyte-SFM culture medium (37010-022, Invitrogen supplied with prequalified human recombinant epidermal growth factor 1-53 [EGF 1-53], bovine pituitary extract [BPE] and glutamine) supplemented with 2 ng/ml leukemia inhibitory factor (L5283, Sigma), 2 ng/ml stem cell factor (H8416, Sigma), 100 ng/ml cholera toxin, 1 ng/ml granulocyte macrophage colony stimulating factor (CYT-221-A, PROSPEC), and 10% Fetal Bovine Serum (FBS) (Attard et al. 2009).

The two kinds of cancer cell lines were grown in a model environment which resembled the environment of bones or lymph nodes, respectively. The bone environment was developed on a co-cultivation model between Human Osteoblasts (HOb) and the relevant prostate cancer cell line. The Human Osteoblasts (HOb) (C-12720, PromoCell) were isolated from fetal human bones. The cells, responsible for bone mineralization, provided an excellent model system for studies relevant to the skeletal system. It was an adherent cell line cultured in Osteoblast Cell Growth Medium (C-27001, PromoCell).

The lymph nodes were similarly developed on a co-cultivation model between the endothelial cell line (HDLEC) and the relevant prostate cancer cell line. Primary Human Dermal Lymphatic Endothelial Cells (HDLEC) (C-12216, PromoCell) were a subpopulation of the Human Dermal Endothelial Cells. They were isolated from the dermis of juvenile foreskin. Lymphatic vessels transport excess fluids from tissues to the circulatory system and are a major component of the immune system. The transported fluid is nearly cell free. The vessels are highly permeable, because they lack a continuous basal membrane. Lymphatic endothelial cells are involved in pathological alterations of the lymphatic system. During tumor lymphangiogenesis, the lymphatic endothelial cells build new vessels that infiltrate tumors, attract tumor cells, and induce

tumor cell metastasis (He et al. 2021). It was an adherent cell line cultured in Endothelial Cell Growth Medium (ready-to-use) (C-22022, PromoCell).

3D Cultures – Alvetex®

The 3D cell culture was introduced using the Alvetex® technology. This is a highly porous polystyrene scaffold designed for 3D cell culture. Cells grown in Alvetex® possess a natural tissue-like structure that enables them to function in a more physiologically relevant manner. The 3D cell culture enables cells to maintain their *in vivo* morphology, behavior, and responsiveness within an *in vitro* model system. In conventional 2D cell culture, cells come into contact with the flat surface of the culture vessel (e.g. Petri dish, flask or multi-well plate). In this unnatural environment, cells get flattened against the substrate. In this abnormally thin structure, the internal cellular components are significantly re-modelled. The entire cytoskeleton is re-modelled and organelles, such as the nucleus, are flattened. The 3D cell culture technology has been designed to stop this shape change from happening. Cells enter the scaffold, where they retain their natural 3D architecture and do not flatten out like in conventional 2D cell culture technology. Thus, by introducing the vertical dimension, the Alvetex® Scaffold technology allows cells to retain their natural 3D shape, morphology, and organization and helps preserve the natural attributes of the cell. Moreover, this technology not only preserves the native 3D shape of individual cells, it also acts to bring cells together in a more natural manner. This results in the formation of tissue-like structures and cell-to-cell interactions that are more representative of normal tissue function. The Alvetex® scaffold technology enabled more sophisticated investigation and clearly showed the relevance and value of the data generated to researchers wishing to replicate an *in-vivo*-like situation. Thus, it helped them to develop a better understanding of basic biology, the mechanism of drug action, and disease modeling (Edmondson et al. 2016).

The bone environment was developed with 3D cell culture in Alvetex® inserts (AMS.AVP005-96, AMSBIO). Human Osteoblasts (HOb) were plated on the scaffolds in a 6-well plate (07-6006, Biologix) and cultured in 7 ml of Osteogenic Medium. The Osteogenic Medium consisted of HOBs basal medium (C27010, PromoCell) with 10 mM glycerol 2-glycerophosphate (G9422-10G, Sigma-Aldrich), 50 µg/ml L-ascorbic acid (A8960-5G, Sigma-Aldrich), and 100 nM

dexamethasone (D4902-25M, Sigma-Aldrich). The cells were refed two times per week (7 ml) for 21 days. This was followed by a co-culture with prostate cell lines for 5 days in RPMI 1640 culture medium with 2 mM Glutamine, 10% Fetal Bovine Serum (FBS) and 1% hydroxyethyl piperazineethanesulfonic acid (HEPES) after the 21-days-growth of Human Osteoblasts in Osteogenic Medium. HEPES has no nutritional benefit to cells. It is added to the medium solely for extra buffering capacity when cell culture requires extended periods of manipulation outside of a CO_2 incubator. The addition of HEPES provides supplemental buffering to the cell culture medium at pH 7.2 to 7.6 (Baicu and Taylor 2002).

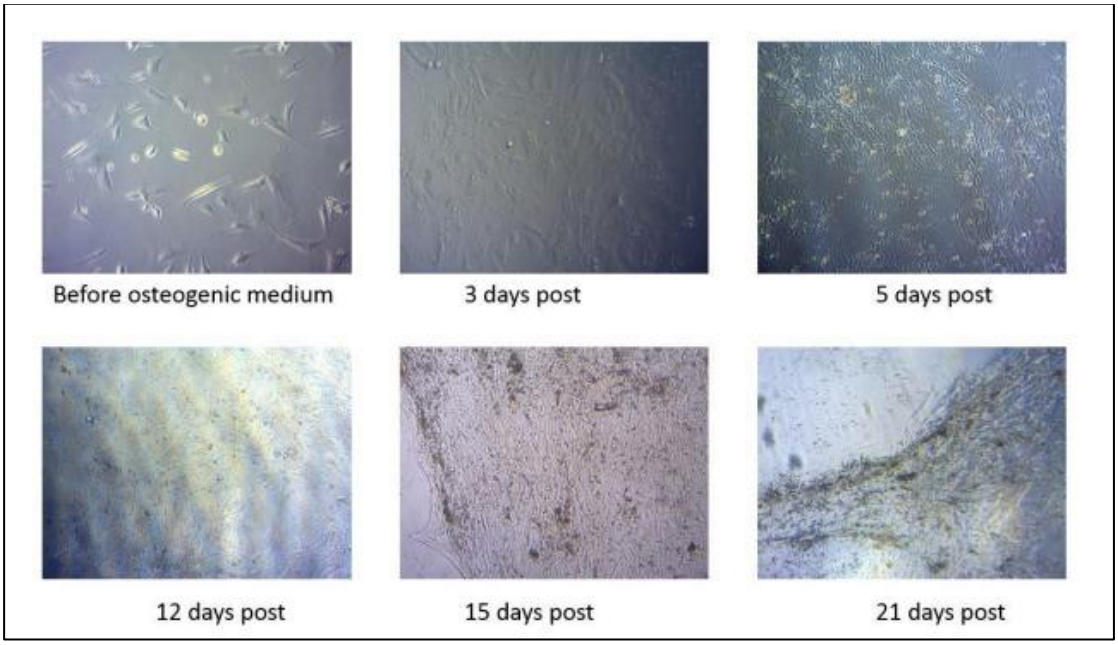

Figure 1: Cell line images under microscope, during culture with osteogenic medium. Cells visualized before addition of osteogenic medium and post-addition of medium at different times (3, 5, 12, 15, and 21 days).

The lymph nodes were similarly developed with 3D cell culture in Alvetex® scaffolds. An endothelial cell line (HDLEC) was plated on the scaffolds in a 6-well plate and cultured in 7 ml Endothelial Cell Growth Medium for 1 day. There followed a co-culture with prostate cell lines for 5 days in RPMI 1640 culture medium with 2 mM Glutamine, 10% FBS, and 1% HEPES. The RNA was isolated from cells with RNeasy Mini Kit for further analysis. The normalization in the data analysis similarly happened with scaffolds plated with endothelial cell line (HDLEC) or with prostate cell lines alone. The co-cultivation of an endothelial cell line (HDLEC) with prostate cell lines without scaffolds was also performed. The process of removing the cells from the scaffolds in order to proceed to RNA isolation was very critical. The membrane of the scaffolds was removed, washed with phosphate-buffered saline, ph 7.4 (PBS) (P3813, Sigma), and

left in 3 ml of trypsin-EDTA 0.25% (T4049-500 ml, Sigma) for 15 minutes at 37 °C. Trypsin-EDTA 0.25% was then inactivated with 3 ml of culture medium and the cells were centrifuged. The supernatant was discarded and the cell pellet was resuspended in culture medium. The cells were then ready for RNA isolation.

3D Cultures – Matrigel®

Parallel to using the Alvetex® scaffold technology, another type of 3D cell culture was employed, the so-called Matrigel®. This is a protein mixture in gelatinous form produced from Engel-Holm-Swarm (EHS) mouse sarcoma cells. Matrigel® resembles the extracellular environment found in many tissues and is used as a substrate for culturing cells. Cells cultured on Matrigel® demonstrate a complex cellular behavior similar to *in vivo* conditions. It can be used in angiogenesis assays to study the networks created by endothelial cells that resemble the microvascular capillary systems, which suffuse living tissues with blood. Tumor growth and metastatic models can also be studied using the Matrigel® technology. The main components of Matrigel® are structural proteins such as laminin, nidogen, collagen, and heparan sulfate proteoglycans, which provide cultured cells with the adhesive peptide sequences that they would encounter in their natural environment. Also present are growth factors like TGF-beta and EGF, which prevent differentiation and promote the proliferation of many cell types.

Much like Alvetex® scaffolds technology, Matrigel® technology allows cells to retain their natural 3D morphology and organization, thus preserving their natural attributes. Unlike Alvetex® technology, Matrigel® is transparent and ideal for imaging the cells during the assays. It also makes it easier to dissolve and recover the cells for downstream applications. For the Matrigel® 3D cell co-cultures, different numbers of cancer cells from each of the different conditions to be tested were mixed with endothelial cells. The cell mix was resuspended in Matrigel®-RPMI mix (ratio 1:1) and plated in the center of the wells of 24 well plates. Plates were incubated at 37 °C for 30 minutes in order to let the Matrigel® solidify. After 30 minutes, 1 ml of RPMI medium containing 1 µg/ml tetracyclin was slowly added into the cultures. The cells were co-cultured for 4 days before RNA extraction. In order to recover the cells, the Matrigel® co-culture had to be broken down. This was achieved by incubating the plates at 4 °C for 1 hour. This allowed the Matrigel® to liquify, while having little to no effect on cell viability. After

1 hour, the 3D culture was dissolved into the medium by gently pipetting each well several times. The medium was removed and the wells were washed with ice-cold PBS to ensure minimal cell loss. After that the cells were ready for RNA extraction.

Calcium Detection

The harvesting period was calculated based on the calcium release by osteoblasts. The osteoblasts 3D cell culture calcium detection in supernatants of co-cultures was performed by EDTA titration. EDTA binds on Ca with higher affinity than Mg. On the other hand, Eriochrome Black T (CL00.0510.0010, Chem-Lab) binds on Mg with higher affinity than Ca and is blue under basic conditions and red when in a complex with Mg. The addition of EDTA (LN40074-A-14, LachNer) reduces free Ca and Mg in the solution. When EDTA binds the Mg from Eriochrome Black T, the solution turns blue (MTSU n. d.). Titration results revealed that calcium was released from the start of co-cultivation. The highest concentrations occurred between day 3 and day 6 and we selected day 5 for the harvesting of co-cultures.

Flow Cytometry

All cell lines were initially (before co-culture) tested for Prostate-Specific Membrane Antigen (PSMA). The hormone-refractory cell lines (PC3, DU145, and SerBob) were not supposed to express PSMA, while hormone-sensitive cell lines (LNCaP, VCaP, and MDA-PCa-2b) were expected to express higher levels of PSMA. For PSMA expression, mouse anti-human PSMA antibody was used, conjugated with Phycoerythrin (AbCam, AB77228). The cells were trypsinized, washed in PBS-2% BSA buffer, and stained using the concentration of antibody suggested by the manufacturer. The cells were incubated for 20 minutes and then washed with PBS-2% BSA. Then they were centrifuged for 5 minutes at 1600 rpm and the pellet was resuspended in 500 ul of phosphate buffered saline. Data acquisition was performed on a Becton Dickinson FACS Calibur equipped with 2 lasers (blue, red) and data analysis was performed using FCSExpress v6. Gates were drawn using the negative samples on FL2-SS dot plots for PSMA expression.

MYO1B, MYADM, and PIP5K1a expression was tested on clinical and healthy blood samples. Monoclonal antibodies conjugated with fluorescein (FITC) were used against the above three proteins. 100 µl of blood were stained with each of the monoclonal antibodies. Then the samples were fixed and permeabilized in order to expose the intracellular epitopes. The staining protocol was as above and samples were analyzed on a Becton Dickinson FACS Calibur equipped with 2 lasers (blue, red). Data analysis was performed using FCSExpress v6. Gates were drawn using the control (unstained) samples on FL1 histograms for FITC expression.

DNA Microarrays

The total RNA from cultured cells was extracted using an RNeasy Mini Kit (74105; Qiagen, Hilden, Germany). A total of 1 µg of the extracted RNA was prepared for DNA microarray experiments using the Amino Allyl MessageAmps II kit (AM1753; Ambion, TX, USA) according to the manufacturer's protocol. The dye was performed by using the Amersham CyDye Post-labelling Reactive Dye Pack (RPN5661; GE Healthcare, UK). The reference sample was labeled with Cy3, while the prostate samples were labeled with Cy5. For each condition, the reference and prostate samples were mixed together and hybridized on a Human Ready Array platform (HS1100; Microarrays Inc., AL, USA). The pre-hybridization, hybridization and washing procedures were automated on the HS400Pro (TECAN, Switzerland). Finally, the slides were imaged on the InnoScan 710 scanner (Innopsys, France) with 5 µM resolution. Scanned microarray image data were used to process expression data by Array-Pro Analyzer 6.3 Software. The microarray gene expression data were normalized using background subtraction.

Real-time qPCR

The total RNA samples (1 µg) were used as a template for cDNA synthesis using a PrimeScript RT Reagent Kit (RR037A; Takara, Beijing, China). Real-time qPCR was then performed using KAPA SYBR Fast Master Mix (2×) Universal (KK4618; KAPA Biosystems, MA, USA) in a final volume of 20 µl. Specific primers for each marker and for reference genes were designed using Beacon Designer 8. Primer sequences were evaluated by BLAST aiming to exclude those that would amplify undesired genes (**Tab. 1**). The PCR program was as follows: initial denaturation at 95 °C for 2 min followed by 45 cycles of denaturation at 95 °C for 10 s and annealing at 59 °C

for 30 s. A melting-curve analysis was performed from 70 °C to 90 °C with 0.5 °C increments for 5 s at each step. The DeltaCt (ΔCt) value was used for analysis of the experiments. The ΔCt calculates the relative expression of a gene of interest in relation to another gene.

In all sets of reactions, cDNA from Universal Human Reference RNA (740000-41; Agilent, CA, USA) was used as a positive control. Template-free and negative controls were also used in all experiments. All the reactions were performed in triplicates.

Table 1: Primer sequences for all the primers tested with RT-qPCR. ACTB represents the housekeeping gene actin-β.

Gene	Forward Primer (5'–3')	Reverse Primer (5'–3')
ACTB	GCCCTGGACTTCGAGCAAGAGA	CAGGAAGGAAGGCTGGAAGAGTG
MYADM	CCACCATCACAACCACCAC	TAGCCACCAGCGAGAAGG
SPAG9	ATGTATCTACTGGCTCTGCTGAA	TTTGGTGGGAGTGCTTGAAC
FGF7	GGAGGGGATATAAGAGTGAGAAGAC	ATTATTCTTCATCTCTTGGGTCCCT
PIP5K1A	CTGTTGCCTTCCGCTACTTC	TCGTCGCTGGACACATAGAATA
SSX2IP	TGCTTCACCTTCCACTTCAGA	TCTTGACGCCACACTCCAT
PTGER4	GGAAGACACCACCTCACTGA	ACCAGCCTCATCCACCAG
OCLN	CTTCGCCTGTGGATGACTTC	CTTGCTCTGTTCTCTTTGACCTT
KLK15	GCTGGAAGGTGACGAGTGT	GTGTGGGGAGATGAGGGAAG
MYO1B	ACAGCCAAGAGGTGAAAGAAAC	GCCGAATCCAGACTCAGGTA
PRDM4	CAATAGACTCTCGCTCTGTGAAC	TCCTCTGCCATTCCATCTGT

Transient Knockdown Experiments

During the exponential phase of proliferation, cells were plated in 12-well plates (4430400N; Orange Scientific) and transfected with gene-specific siRNAs using Xfect RNA Transfection Reagent (631450; Takara), according to the manufacturer's instructions. The siRNA molecules were designed in accordance with the rules of Reynolds et al. (2004).

The siRNA sequences were as follows (**Tab. 2**):

Table 2: siRNA sequences for permanent KD assays. All siRNA molecules added as double-stranded RNA molecules, with a dTdT overhang at 3'.

Gene	Sequence (5'-3')
SPAG9	AGAUCUCAGUGGAUAUAAA-dTdT
	UUUAUAUCCACUGAGAUCU-dTdT
MYADM	GGCAACUGGUCCAUGUUCA-dTdT
	UGAACAUGGACCAGUUGCC-dTdT
PIP5K1A	GACGAUGAGUUCAUUAUUA-dTdT
	UAAUAAUGAACUCAUCGUC-dTdT
PTGER4	GAAAGACAGUGCUCAGUAA-dTdT
	UUACUGAGCACUGUCUUUC-dTdT
MYO1B	GGAUAUGGUUCUUUUAGAA-dTdT
	UUCUAAAAGAACCAUAUCC-dTdT
PRDM4	GCAACCUUGUUUACAAUUU-dTdT
	AAAUUGUAAACAAGGUUGC-dTdT

All sequences were run on BLAST to ensure there was no risk of off-target effects. After 48 h of incubation, the cells were harvested by trypsinization (T4049; Sigma-Aldrich). For each condition, samples were incubated with Xfect Reagent only (without siRNA), in order to study the effect of the Xfect Reagent itself on gene expression. Finally, samples incubated with non-specific siRNA were tested to study the specificity of the particular siRNA. The mRNA knockdown was calculated relative to a non-targeting control siRNA in each experiment. The expression level of the gene of interest and its percentage knockdown were calculated using the comparative Ct method (Livak and Schmittgen 2001):

$\Delta Ct = Ct_{target} - Ct_{ACTB}$

$\Delta\Delta Ct = \Delta Ct_{(siRNA\ treated)} - \Delta Ct_{(siRNA\ non\text{-}treated)}$

Relative expression level = $2^{-\Delta\Delta Ct}$

% KD = $100 \times (1-2^{-\Delta\Delta Ct})$

Stable Knockdown Experiments

In order to create stable KD on cells, the BLOCK-iT™ Inducible H1 RNAi Entry Vector Kit (K492000; Thermofisher Scientific) was used. The sequences for shRNA were based on previous siRNA molecules (**Tab. 3**).

Table 3: Sequences for shRNA (forward and reverse) used for the creation vectors.

Gene	Sequence (5'-3')
SPAG9	CACCagatctcagtggatataaCGAAtttatatccactgagatc
	AAAAagatctcagtggatataaaTTCGtttatatccactgagatc
MYADM	CACCggcaactggtccatgttcaCGAAtgaacatggaccagttgccC
	AAAAGggcaactggtccatgttcaTTCGtgaacatggaccagttgcc
PIP5K1A	CACCgacgatgagttcattattaCGAAtaataatgaactcatcgtcC
	AAAAGgacgatgagttcattattaTTCGtaataatgaactcatcgtc
PTGER4	CACCgaaagacagtgctcagtaaCGAAttactgagcactgtctttcC
	AAAAGgaaagacagtgctcagtaaTTCGttactgagcactgtctttc
MYO1B	CACCggatatggttcttttagaaCGAAttctaaaagaaccatatccC
	AAAAGggatatggttcttttagaaTTCGttctaaaagaaccatatcc
PRDM4	CACCgcaaccttgtttacaatttCGAAaaattgtaaacaaggttgcC
	AAAAGgcaaccttgtttacaatttTTCGaaattgtaaacaaggttgc

The cloning and transfection were performed according to the manufacturer's instructions, using competent cells appropriate for the above assays. The isolated recombinant DNA was used to transform prostate cancer cell lines with Xfect (631317; Takara). Cells were selected with Zeocin™ Selection Reagent (R25001; Thermofisher Scientific) and then co-cultured with endothelial cells.

In positive knockdown cells, genes correlated with metastasis, invasion, and endothelial-mesenchymal transition were analyzed by qRT-PCR. The analyzed genes included CD44, Cadherin-1 (CDH1), N-cadherin (CDH2), Catenin beta-1 (CTNNB1), Dipeptidyl peptidase-4 (DPP4), Integrin alpha-5 (ITGA5), Integrin alpha-V (ITGAV), Integrin beta-1 (ITGB1), Integrin beta chain-2 (ITGB2), cytokeratin-19 (KRT19), Zinc finger protein SNAI1 (SNAI1), Zinc finger protein SNAI2 (SNAI2), Twist-related protein 1 (TWIST1), Caveolin-2 (CAV2), Claudin 3 (CLDN3), epidermal

growth factor receptor (EGFR), Desmocollin-1 (DSC1), Fibronectin (FN1), hepatocyte growth factor receptor (MET), Epithelial cell adhesion molecule (EPCAM), and Vimentin (VIM).

Statistical Analysis

ANOVA (Analysis of Variance) tests the hypothesis that all group means are equal versus the alternative hypothesis that at least one group mean is different from the others. In particular, the procedure assigns sample variance to different sources and decides whether the variation arises within or among different population groups. Samples are described in terms of variation around group means and variation of group means around an overall mean. If variations within groups are small relative to variations between groups, a difference in group means may be inferred (Schober and Vetter 2020).

In this data set, ANOVA treats each column as a separate group and evaluates whether the population means of the columns are equal. If the test hypothesis in ANOVA – i.e. that all group means are equal – is rejected, we can determine which group means are different from others. In particular, a pairwise comparison results from a multiple comparison test using the Bonferroni method (Armstrong 2014). Then, a p-value is estimated (p-value for testing the hypothesis that the corresponding mean difference is equal to zero) concerning the comparison of each group with another group. Values lower than 0.05 (or 0.01) indicate the significance of the difference between group means. The statistical analysis was performed using MATLAB.

This was followed by Tukey's Q pairwise test using PAST statistical software, in order to evaluate the gene expression change between the cell lines cultured with osteoblasts and endothelial cells (Hammer et al. 2001).

Results

PSMA Expression

Initially, cell lines were tested for PSMA expression. The results show (**Fig. 2**) that hormone-sensitive cell lines (LNCaP, MDA-PCa-2b, and VCaP) express PSMA at various levels, as

expected. On the other hand, hormone-refractory cell lines (PC3, DU145, and SerBob) show little to no PSMA expression (Laidler et al. 2005).

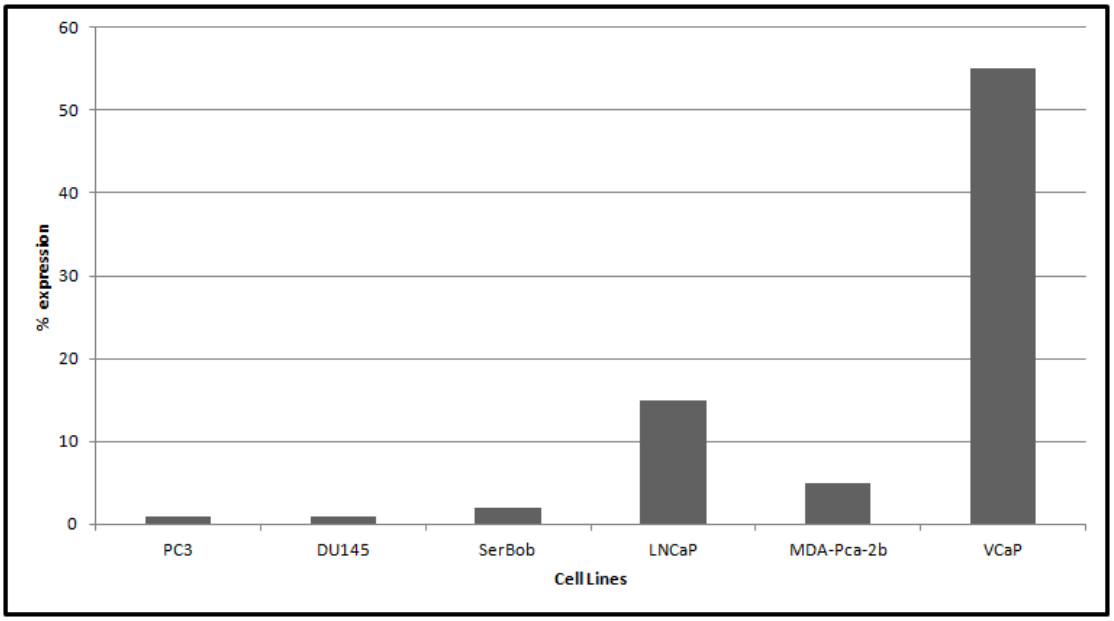

Figure 2: PSMA expression in different prostate cancer cell lines.

Biomarkers Detection

Microarray experiments revealed hundreds of differentially-expressed genes when co-cultivated with osteoblasts or endothelial cells (**Fig. 3**). We also compared gene expression between co-cultivated cells, osteoblasts, endothelial cells, and cancer cell lines. Genes highly expressed before co-cultivation were not included in the final analysis.

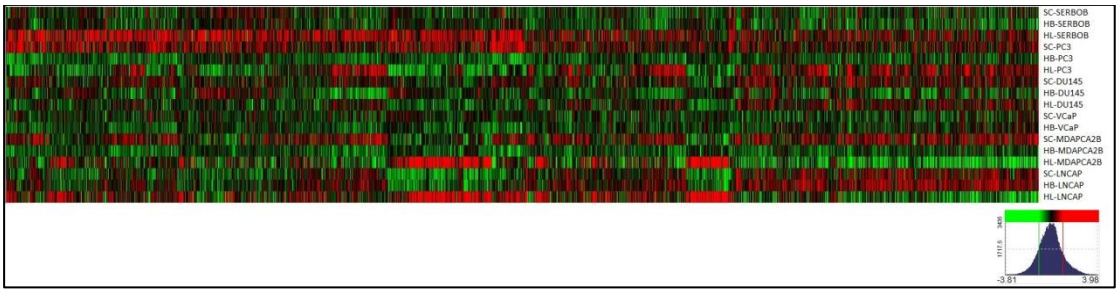

Figure 3: Heatmap of microarray gene expression assays.

After validating the differentially-expressed genes, MYADM, PIP5K1A, PTGER4, MYO1B, SPAG9, OCLN, PRDM4, SSX2IP, KLK15, and FGF7 were selected for further experiments. These were expressed in the initial cancer cell line (before co-cultivation) and had different expression profiles after culture. The figures below (**Fig. 4–13**) illustrate the gene expression levels, calculated according to reference RNA. Positive values indicate overexpression correlated

with the reference RNA, while negative values indicate downregulations relative to reference RNA. The Y-axis represents the log10 value of relative gene expression.

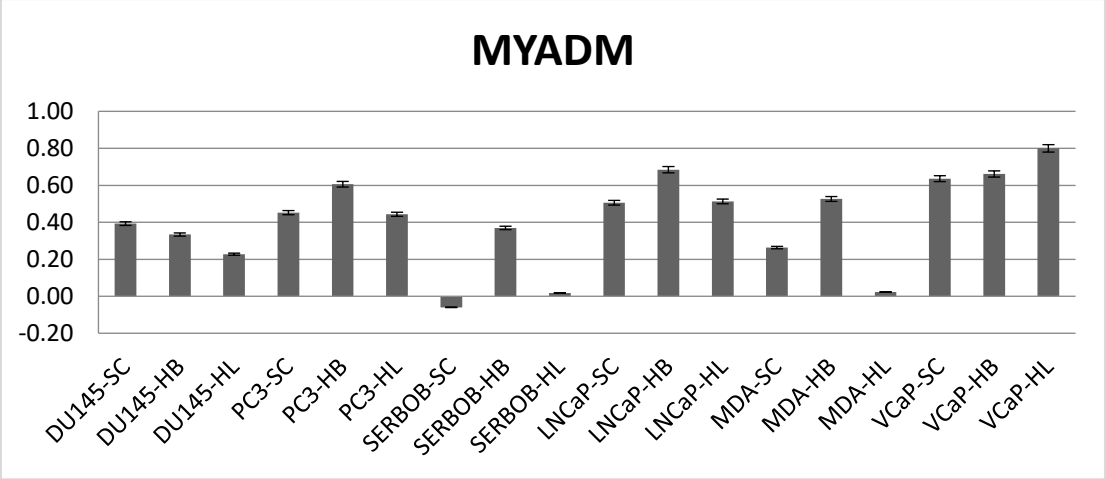

Figure 4: MYADM gene expression in all six prostate cell lines, in 3D cultures themselves (SC), and as co-culture with osteoblasts (HB) or endothelial cells (HL).

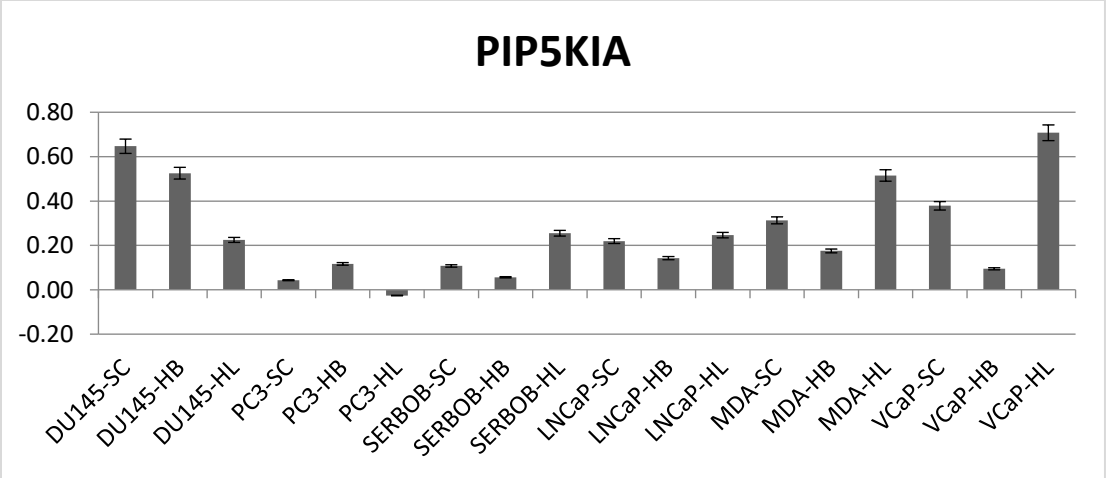

Figure 5: PIP5K1A gene expression in all six prostate cell lines, in 3D cultures themselves (SC), and as co-culture with osteoblasts (HB) or endothelial cells (HL).

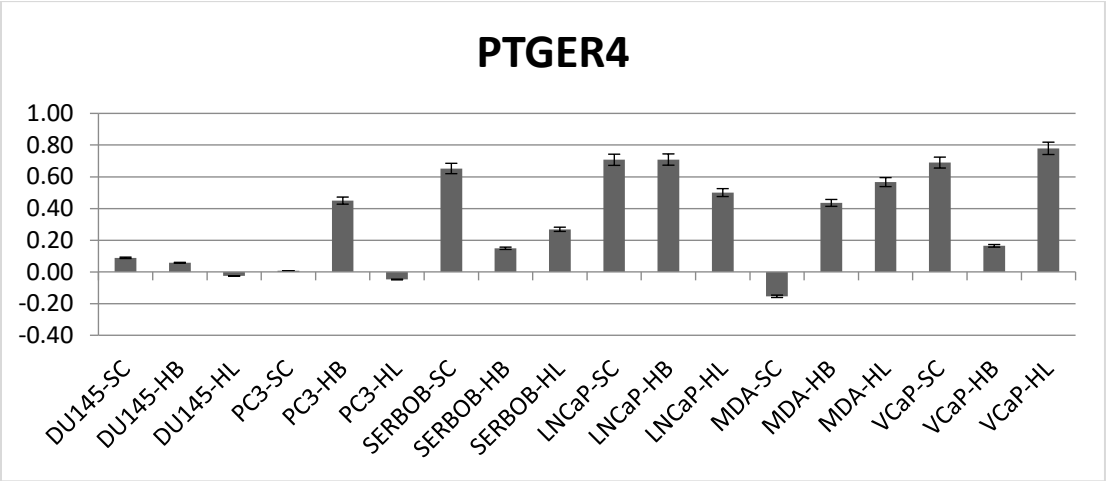

Figure 6: PTGER4 gene expression in all six prostate cell lines, in 3D cultures themselves (SC), and as co-culture with osteoblasts (HB) or endothelial cells (HL).

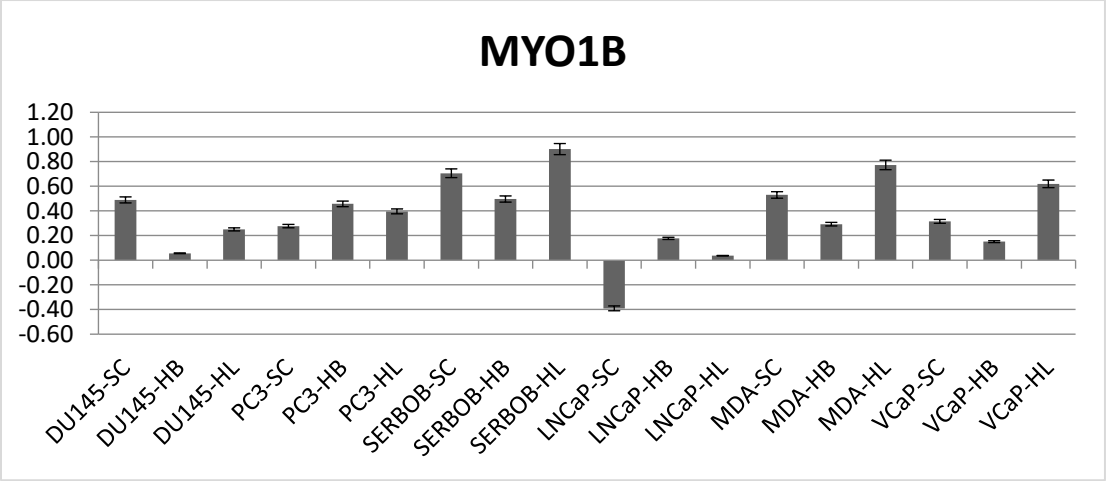

Figure 7: MYO1B gene expression in all six prostate cell lines, in 3D cultures themselves (SC), and as co-culture with osteoblasts (HB) or endothelial cells (HL).

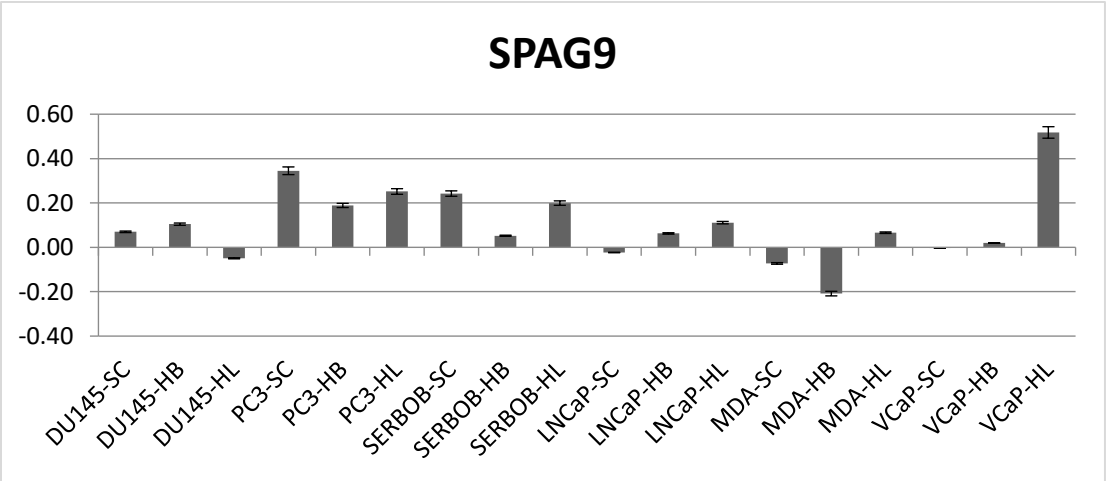

Figure 8: SPAG9 gene expression in all six prostate cell lines, in 3D cultures themselves (SC), and as co-culture with osteoblasts (HB) or endothelial cells (HL).

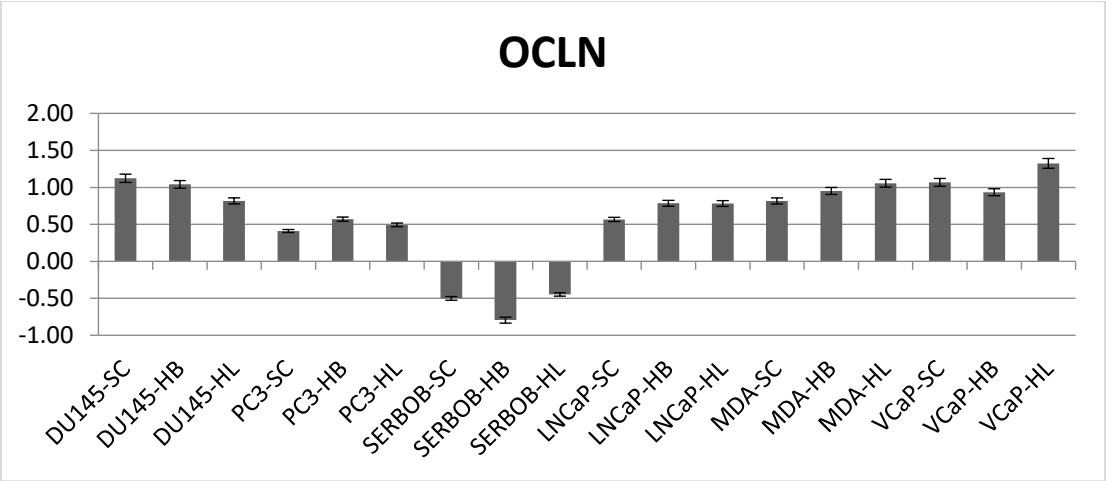

Figure 9: OCLN gene expression in all six prostate cell lines, in 3D cultures themselves (SC), and as co-culture with osteoblasts (HB) or endothelial cells (HL).

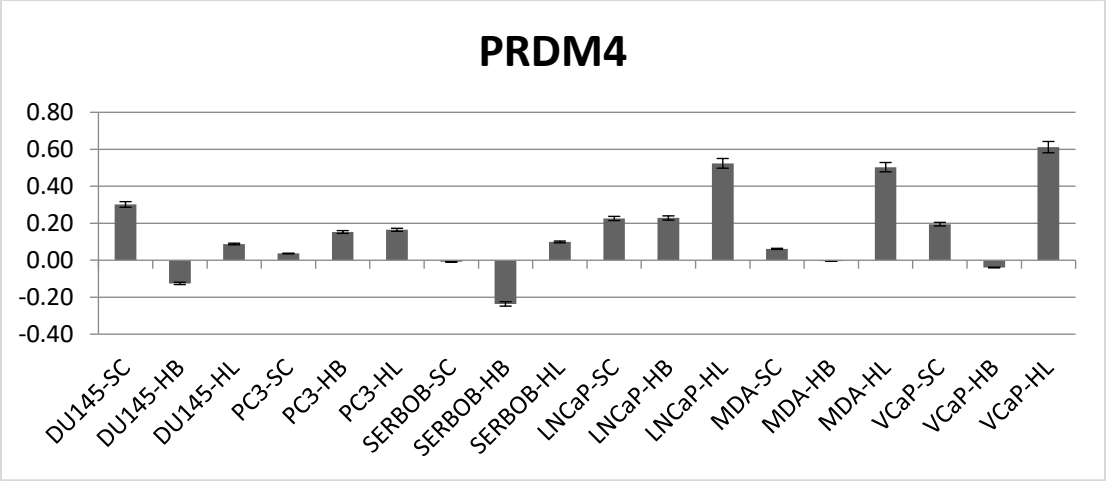

Figure 10: PRDM4 gene expression in all six prostate cell lines, in 3D cultures themselves (SC), and as co-culture with osteoblasts (HB) or endothelial cells (HL).

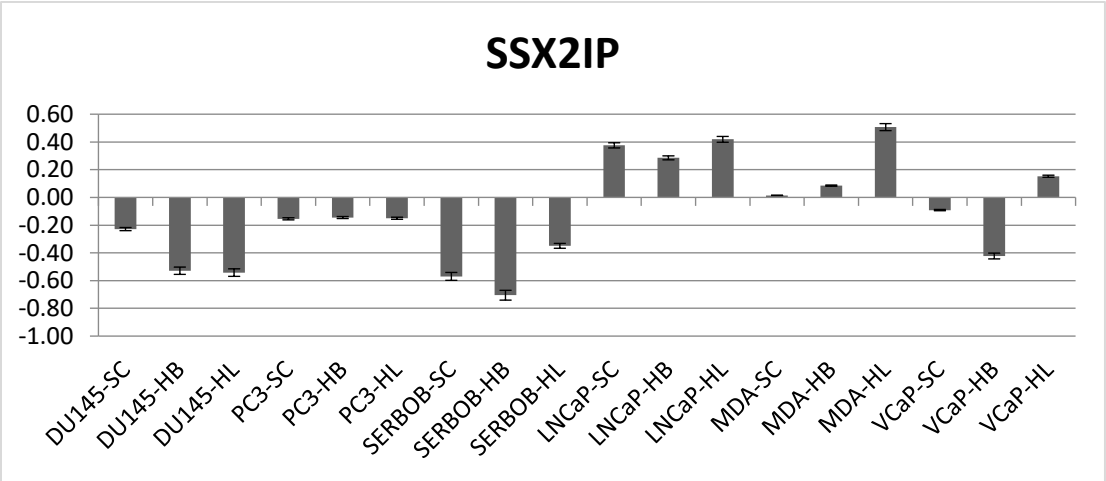

Figure 11: SSX2IP gene expression in all six prostate cell lines, in 3D cultures themselves (SC), and as co-culture with osteoblasts (HB) or endothelial cells (HL).

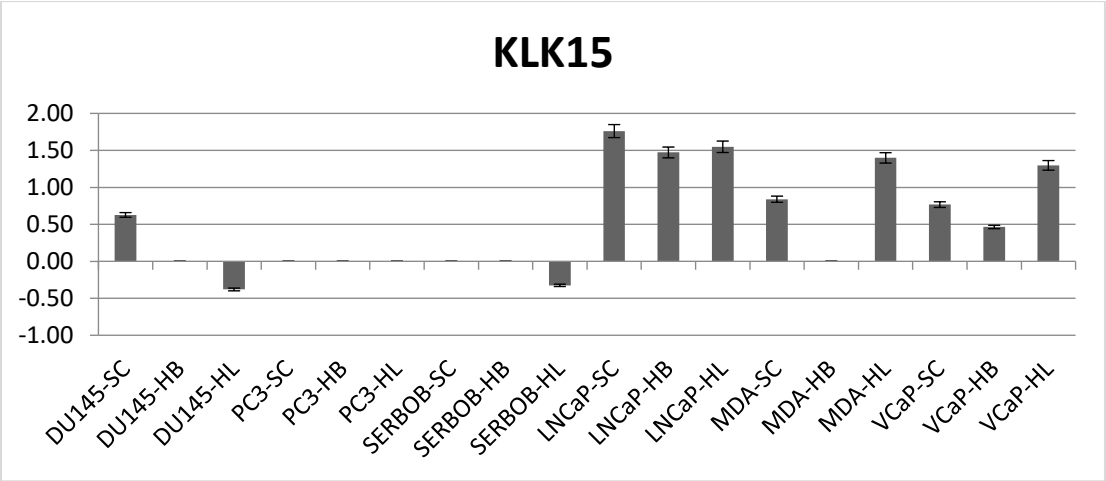

Figure 12: KLK15 gene expression in all six prostate cell lines, in 3D cultures themselves (SC), and as co-culture with osteoblasts (HB) or endothelial cells (HL).

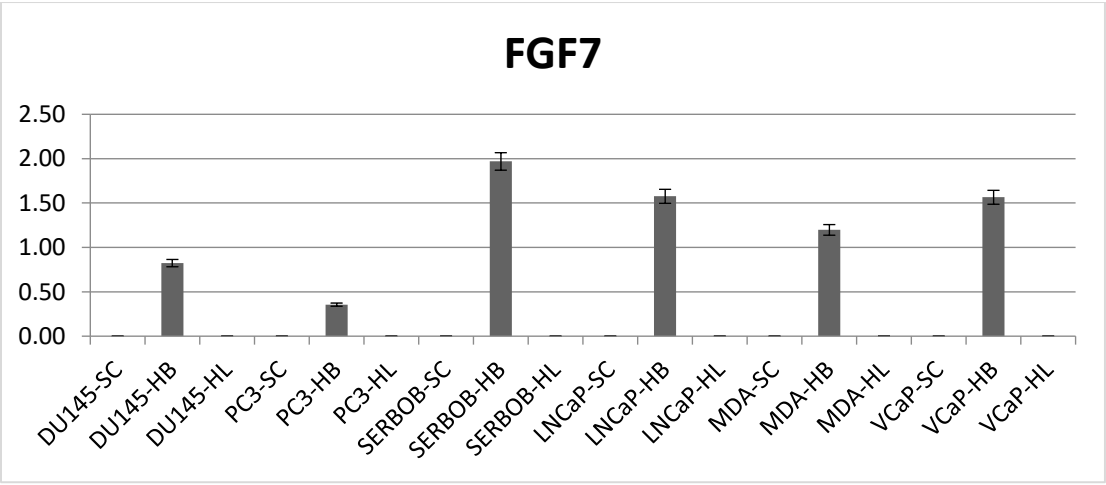

Figure 13: FGF7 gene expression in all six prostate cell lines, in 3D cultures themselves (SC), and as co-culture with osteoblasts (HB) or endothelial cells (HL).

The genes that were finally selected are MYADM, PIP5K1A, and MYO1B (**Fig. 14**), as we observed that only these genes were expressed in the initial cell lines. Moreover, their expression

changed in a different manner depending on whether the cell line was co-cultured with osteoblasts or endothelial cells.

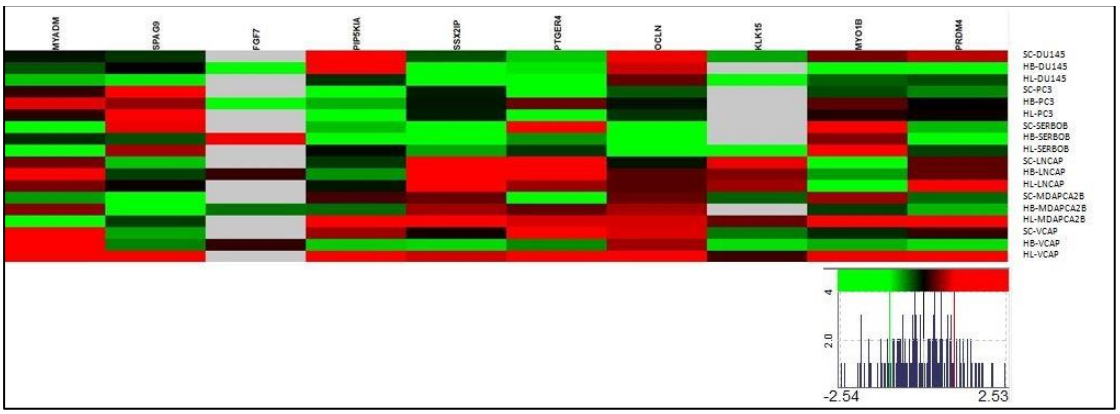

Figure 14: Heatmap of RT-qPCR experiments for selected genes.

The statistical analysis data, based on qPCR gene expression data of all the above markers, revealed that sensitive and refractory cell lines have different profiles when cultivated with endothelial cells. The p value in all cases was <0.05. On the contrary, no significant difference was observed for cells cultivated with osteoblasts.

Therefore, the study then focused on MYADM, MYO1B, and PIP5K1A, which gave the most encouraging data. For these three genes, no significant difference could be observed between the insensitive and sensitive cell lines, in both co-cultures. However, on osteoblasts co-cultivation, the expression pattern of each gene was different (MYADM-PIP5K1A p=0.0078, MYADM-MYO1B p=0.049). No similar difference was observed in endothelial culture.

Regarding the statistical significance among the cultures with endothelial cells and osteoblasts, the tables below (**Tab. 4–6**) present the p value for each pair. In the majority of cases, the gene expression profile is statistically significant between two different conditions of co-cultivation (highlighted values indicate p<0.05).

Table 4: MYADM gene expression statistical analysis.

	PC3-HB	PC3-HL	SERBOB-HB	SERBOB-HL	DU145-HB	DU145-HL	VCaP-HB	VCaP-HL	LNCaP-HB	LNCaP-HL	MDA-HB	MDA-HL
PC3-HB		0.0001429	0.0001429	0.0001429	0.0001429	0.0001429	0.001124	0.0001429	0.0001429	0.0001429	0.0001453	0.0001429
PC3-HL	21.54		0.0001429	0.0001429	0.0001429	0.0001429	0.0001429	0.0001429	0.0001429	0.0001809	0.0001436	0.0001429
SERBOB-HB	77.5	55.97		1	0.0001429	0.0001429	0.0001429	0.0001429	0.0001429	0.0001429	0.0001429	1
SERBOB-HL	78.04	56.5	0.5318		0.0001429	0.0001429	0.0001429	0.0001429	0.0001429	0.0001429	0.0001429	1
DU145-HB	36.03	14.49	41.48	42.01		0.0001429	0.0001429	0.0001429	0.0001429	0.0001429	0.0001429	0.0001429
DU145-HL	50.12	28.58	27.39	27.92	14.09		0.0001429	0.0001429	0.2722	0.0001429	0.0001429	0.0001429
VCaP-HB	7.445	28.98	84.95	85.48	43.47	57.56		0.0001429	0.0001429	0.0001429	0.0001429	0.0001429
VCaP-HL	25.66	47.19	103.2	103.7	61.68	75.78	18.21		0.0001429	0.0001429	0.0001429	0.0001429
LNCaP-HB	53.97	32.44	23.53	24.06	17.95	3.855	61.42	79.63		0.0001429	0.0001429	0.0001429
LNCaP-HL	12.36	9.173	65.14	65.67	23.66	37.75	19.81	38.02	41.61		0.9686	0.0001429
MDA-HB	10.5	11.03	67	67.53	25.52	39.62	17.95	36.16	43.47	1.861		0.0001429
MDA-HL	77.24	55.7	0.2659	0.7976	41.21	27.12	84.68	102.9	23.26	64.87	66.74	

Table 5: MYO1B gene expression statistical analysis.

	PC3-HB	PC3-HL	SERBOB-HB	SERBOB-HL	DU145-HB	DU145-HL	VCaP-HB	VCaP-HL	LNCaP-HB	LNCaP-HL	MDA-HB	MDA-HL
PC3-HB		0.0002384	0.0001429	0.0001429	0.0001429	0.0001429	0.0001429	0.0001429	0.0001429	0.0001429	0.0001429	0.0001429
PC3-HL	8.7		0.0001429	0.0001429	0.0001429	0.0001429	0.0001429	0.0001429	0.0001429	0.0001429	0.0001429	0.0001429
SERBOB-HB	44.07	35.37		0.0001429	0.0001429	0.0001429	1	0.0001429	0.0001429	0.0001429	0.0001429	0.0001429
SERBOB-HL	63.32	72.02	107.4		0.0001429	0.0001429	0.0001429	0.0001429	0.0001429	0.0001429	0.0001429	0.0001429
DU145-HB	56.9	48.2	12.84	120.2		0.0001429	0.0001429	0.0001429	0.0001429	0.7393	0.0001429	0.0001429
DU145-HL	29.38	20.68	14.69	92.7	27.52		0.0001429	0.0001429	0.0001429	0.0001429	0.009663	0.0001429
VCaP-HB	43.5	34.8	0.5705	106.8	13.41	14.12		0.0001429	0.0001429	0.0001429	0.0001429	0.0001429
VCaP-HL	23.1	31.8	67.17	40.22	80.01	52.48	66.6		0.0001429	0.0001429	0.0001429	0.0001429
LNCaP-HB	108.8	100.1	64.75	172.1	51.91	79.44	65.32	131.9		0.0001429	0.0001429	0.0001429
LNCaP-HL	59.61	50.91	15.55	122.9	2.71	30.23	16.12	82.72	49.2		0.0001429	0.0001429
MDA-HB	23.25	14.55	20.82	86.57	33.66	6.132	20.25	46.35	85.57	36.37		0.0001429
MDA-HL	44.64	53.34	88.71	18.68	101.5	74.02	88.14	21.53	153.5	104.3	67.88	

Table 6: PIP5K1A gene expression statistical analysis.

	PC3-HB	PC3-HL	SERBOB-HB	SERBOB-HL	DU145-HB	DU145-HL	VCaP-HB	VCaP-HL	LNCaP-HB	LNCaP-HL	MDA-HB	MDA-HL
PC3-HB		0.0001429	0.0001429	0.0001429	0.0001429	0.0001429	0.7324	0.0001429	0.0001429	0.0001429	0.0008124	0.0001429
PC3-HL	18.43		0.0001429	0.0001429	0.0001429	0.0001429	0.0001429	0.0001429	0.0001429	0.0001429	0.0001429	0.0001429
SERBOB-HB	52.97	34.53		0.0001429	0.0001429	0.0001429	0.0001429	0.0001429	0.00535	0.0001429	0.0001429	0.0001429
SERBOB-HL	17.92	36.35	70.88		0.0001429	0.26	0.0001429	0.0001429	0.0001429	0.9998	0.0001471	0.0001429
DU145-HB	53.1	71.53	106.1	35.18		0.0001429	0.0001429	0.0001429	0.0001429	0.0001429	0.0001429	0.9959
DU145-HL	14.02	32.46	66.99	3.895	39.08		0.0001429	0.0001429	0.0001429	0.6774	0.006623	0.0001429
VCaP-HB	2.726	15.71	50.24	20.64	55.82	16.75		0.0001429	0.0001429	0.0001429	0.000146	0.0001429
VCaP-HL	76.47	94.9	129.4	58.55	23.37	62.44	79.19		0.0001429	0.0001429	0.0001429	0.0001429
LNCaP-HB	59.46	41.02	6.491	77.37	112.6	73.48	56.73	135.9		0.0001429	0.0001429	0.0001429
LNCaP-HL	16.88	35.31	69.84	1.039	36.22	2.856	19.6	59.59	76.34		0.0001777	0.0001429
MDA-HB	7.66	26.09	60.63	10.26	45.44	6.361	10.39	68.81	67.12	9.217		0.0001429
MDA-HL	51.67	70.1	104.6	33.75	1.428	37.65	54.4	24.8	111.1	34.79	44.01	

Biomarkers Evaluation – Transient Knockdown

For the markers showing significant results in qRT-PCR during biomarker detection, knock-down was performed with specific siRNA molecules. The table below (**Tab. 7**) shows the KD efficiency.

Table 7: Percentage of KD experiments (in %). "-" indicates that knockdown was not efficient.

	DU145	PC3	SERBOB	MDA-PCa-2b
MYADM	68.57	69.58	64.25	66.11
PIP5K1A	77.60	63.36	66.07	79.79
PTGER4	33.87	-	-	-
MYO1B	74.65	57.25	61.62	81.92
SPAG9	77.32	66.78	71.78	84.88
PRDM4	58.42	33.02	-	65.58

After KD, qPCR was performed for different markers (**Fig. 15–19**) (all the results are listed in the Raw Data section).

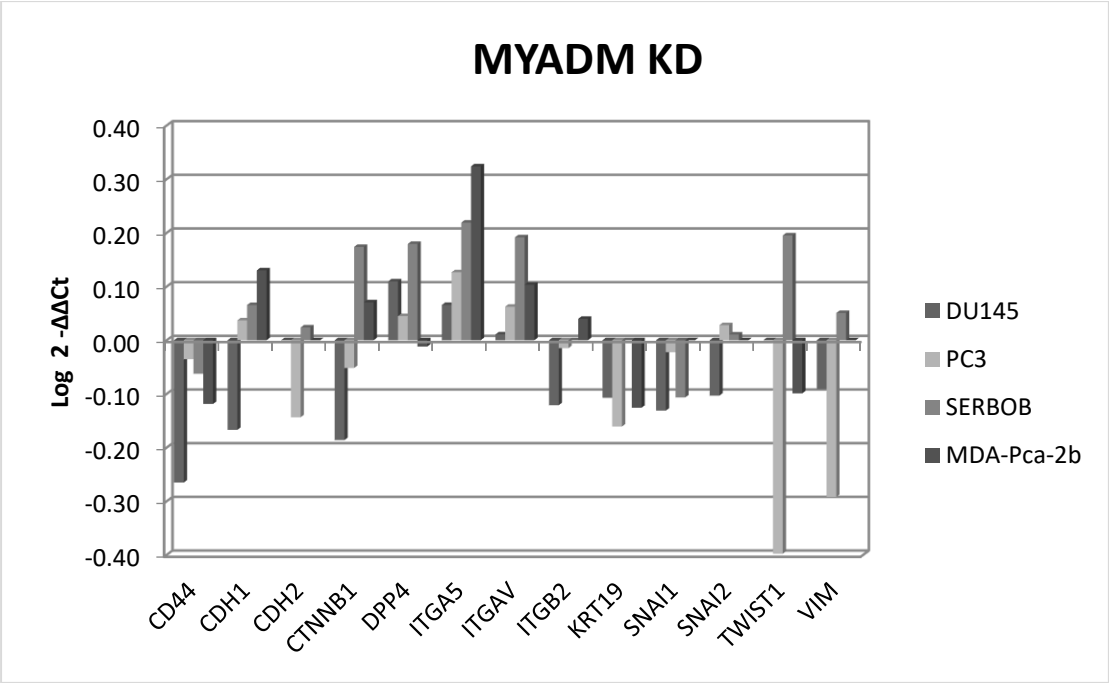

Figure 15: Gene expression post MYADM-KD. Relative quantification performed according to non-KD sample.

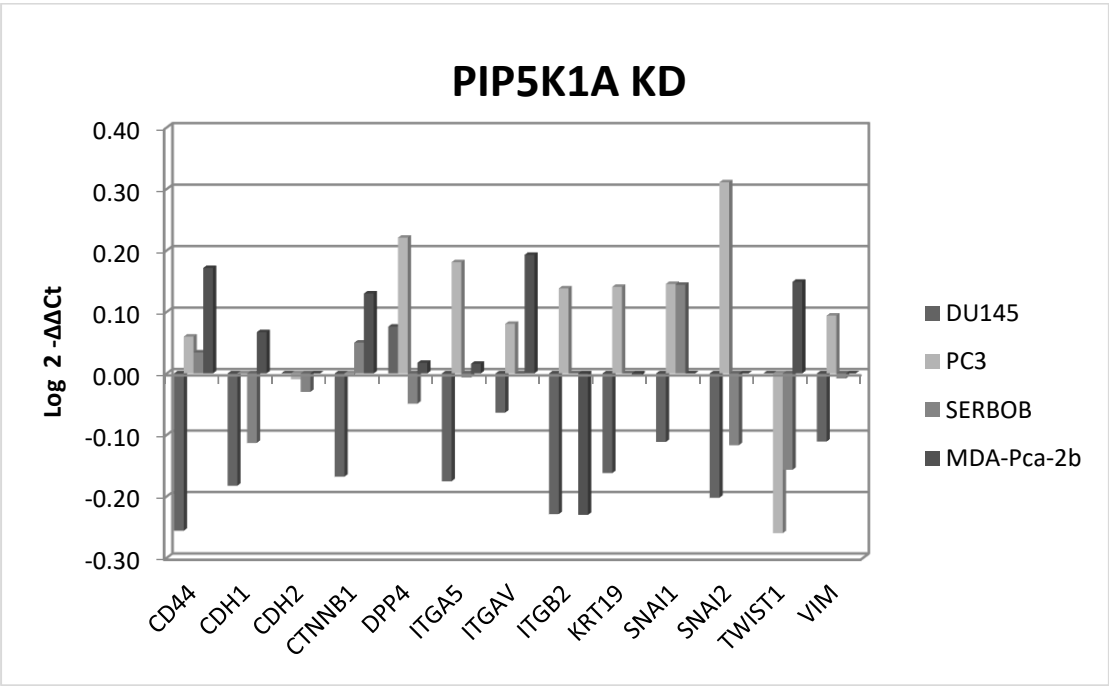

Figure 16: Gene expression post PIP5K1A-KD. Relative quantification performed according to non-KD sample.

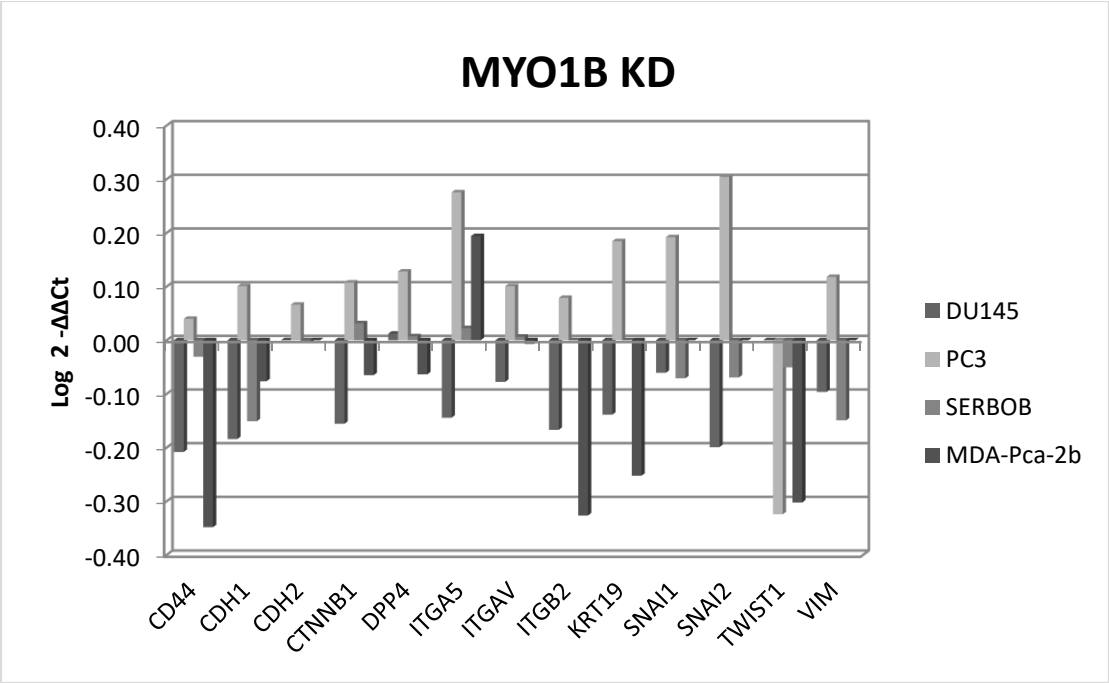

Figure 17: Gene expression post MYO1B-KD. Relative quantification performed according to non-KD sample.

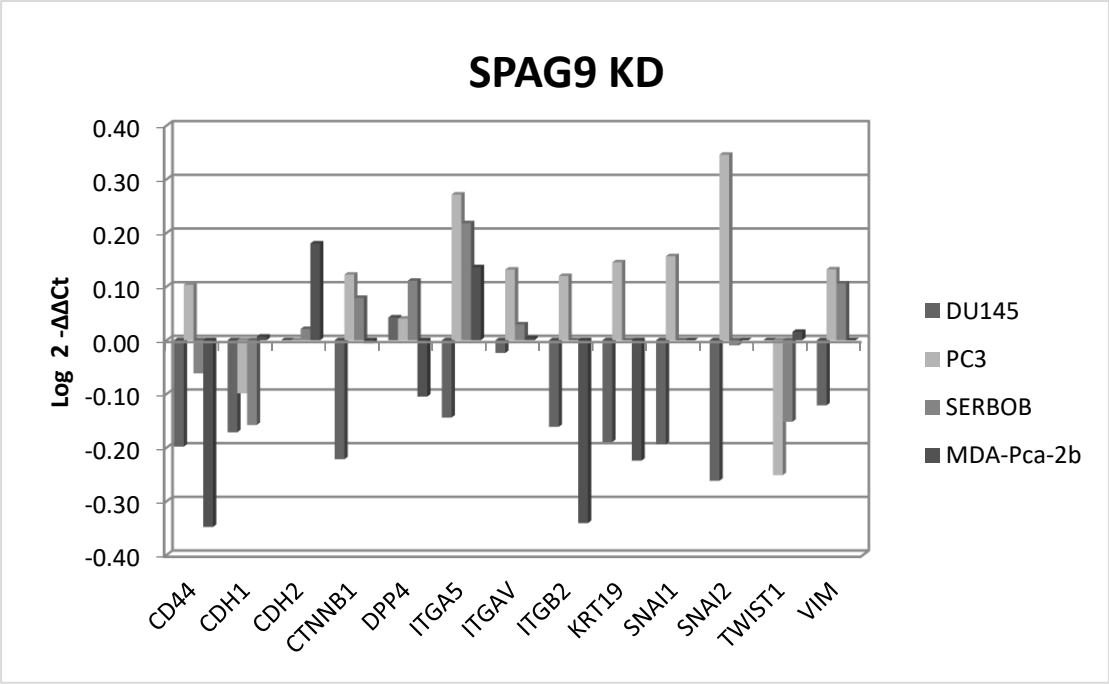

Figure 18: Gene expression post SPAG9-KD. Relative quantification performed according to non-KD sample.

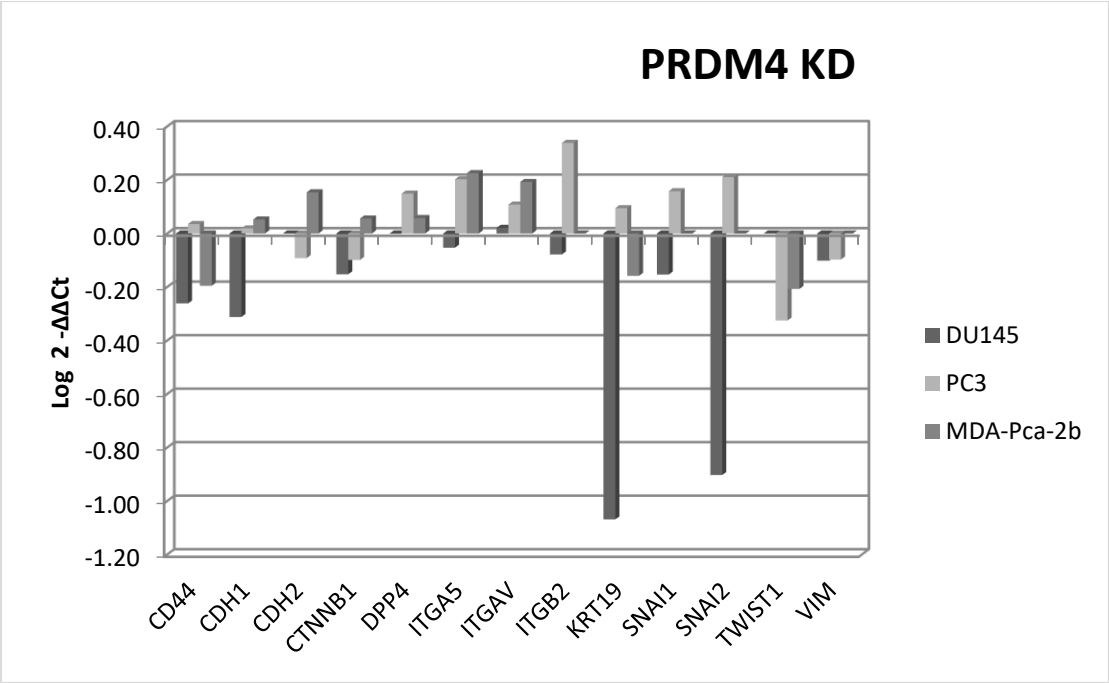

Figure 19: Gene expression post PRDM4-KD. Relative quantification performed according to non-KD sample.

Biomarkers Evaluation – Stable Knockdown

Regarding the stable KD, the shRNA vector was compatible only for MYADM, MYO1B, PIP5K1A, PRDM4, and PTGER4. However, efficient KD was not observed for PRDM4 and PTGER4 in all cell lines. **Table 8** presents the KD efficiency data.

Table 8: Percentage of KD experiments (in %).
N/C: The gene expression decreased and the percentage of KD could not be calculated.

	DU145	PC3	VCaP	LNCaP
MYADM	N/C	N/C	N/C	N/C
MYO1B	25.02	85.9	45.52	-
PIP5K1A	20.77	25.49	69.86	40.45

Following KD, qPCR was performed for different markers (all the results are listed in the Raw Data section). MYADM knockdown caused a decrease in ITGB1, IGF1R, and TWIST1 expression in all cell lines. Further, FN1, ITGA5, ITGAV, and PECAM1 were upregulated in hormone-refractory cell lines, but downregulated in hormone-sensitive cells. MYO1B knockdown downregulated ITGB1 and IGF1R in all tested cell lines and upregulated CTNNB1 and DSC1. We observed MET and PECAM1 overexpression only in hormone-sensitive cell lines. Additionally, ITGB1 and

IGF1R were downregulated after PIP5K1A knockdown. Our results revealed crosstalk between several tested genes, which could explain the expression patterns in some of the associated genes.

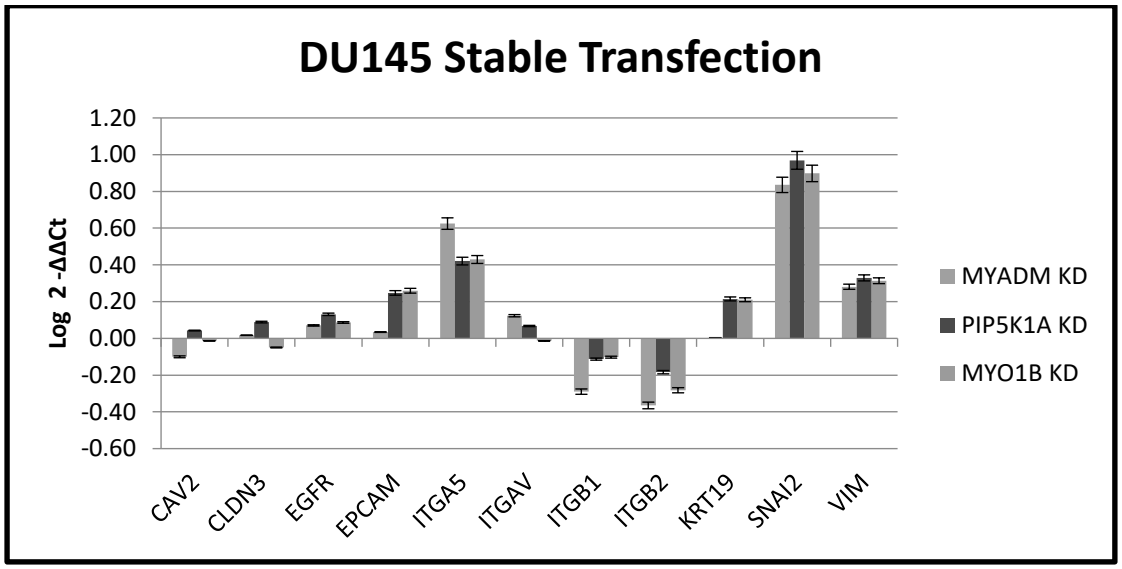

Figure 20: Gene expression post permanent transfection in DU145 prostate cell line.

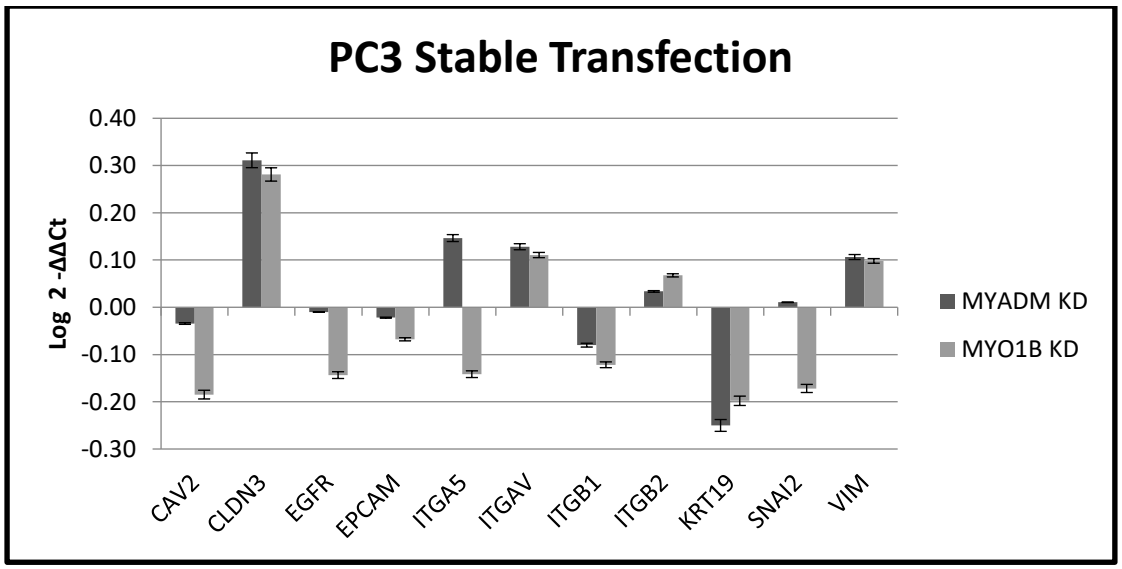

Figure 21: Gene expression post permanent transfection in PC3 prostate cell line.

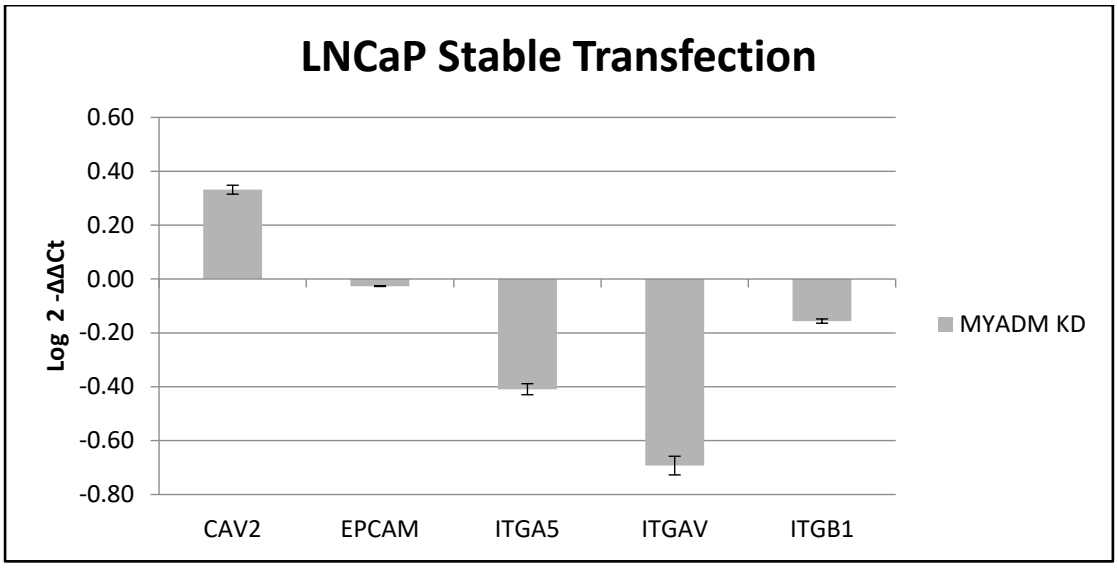

Figure 22: Gene expression post permanent transfection in LNCaP prostate cell line.

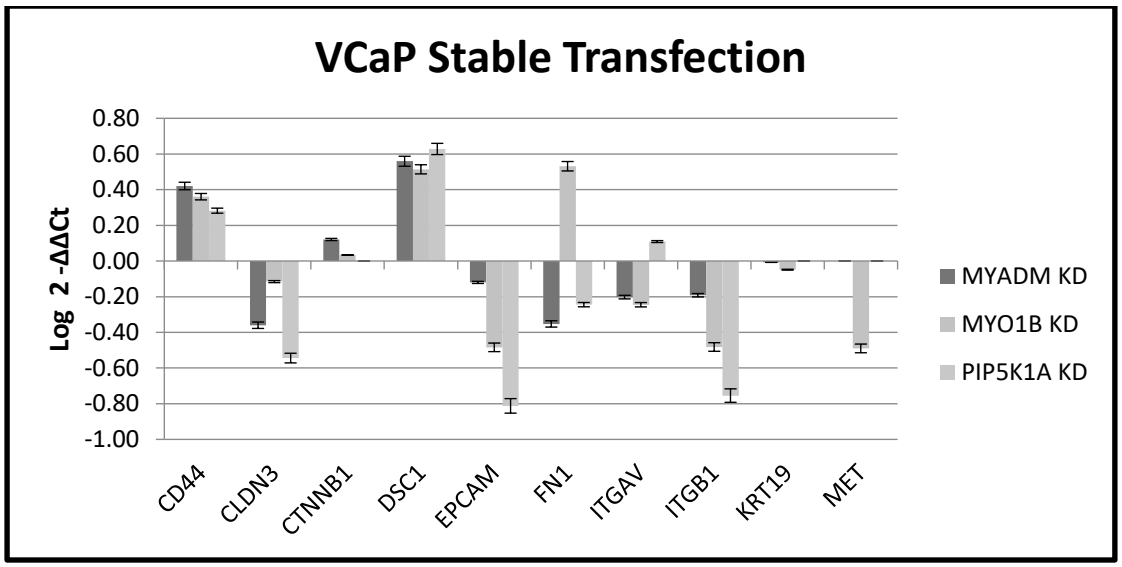

Figure 23: Gene expression post permanent transfection in VCaP prostate cell line.

Cell Lines Co-Cultivation Photos (Stable KD)

We also investigated cellular morphology pre- and post-knockdown of the above specific markers. There were no signs of matrix formation after knockdown (**Fig. 24B**). PC3 cell morphology clearly changed after PIP5K1A knockdown (**Fig. 24B**). We then co-cultivated cells with endothelial cells in Matrigel®. Endothelial tube formation was observed in the co-cultures (**Fig. 24C, 24D**). PC3 control cells appeared to be able to grow close to the human umbilical vein endothelial cells (HUVEC) formations and to form cell clusters (**Fig. 24C**). However, PC3 cells

with PIP5K1A knockdown appeared to grow as single cells without making junctions with other cells or with HUVEC cell formations (**Fig. 24D**).

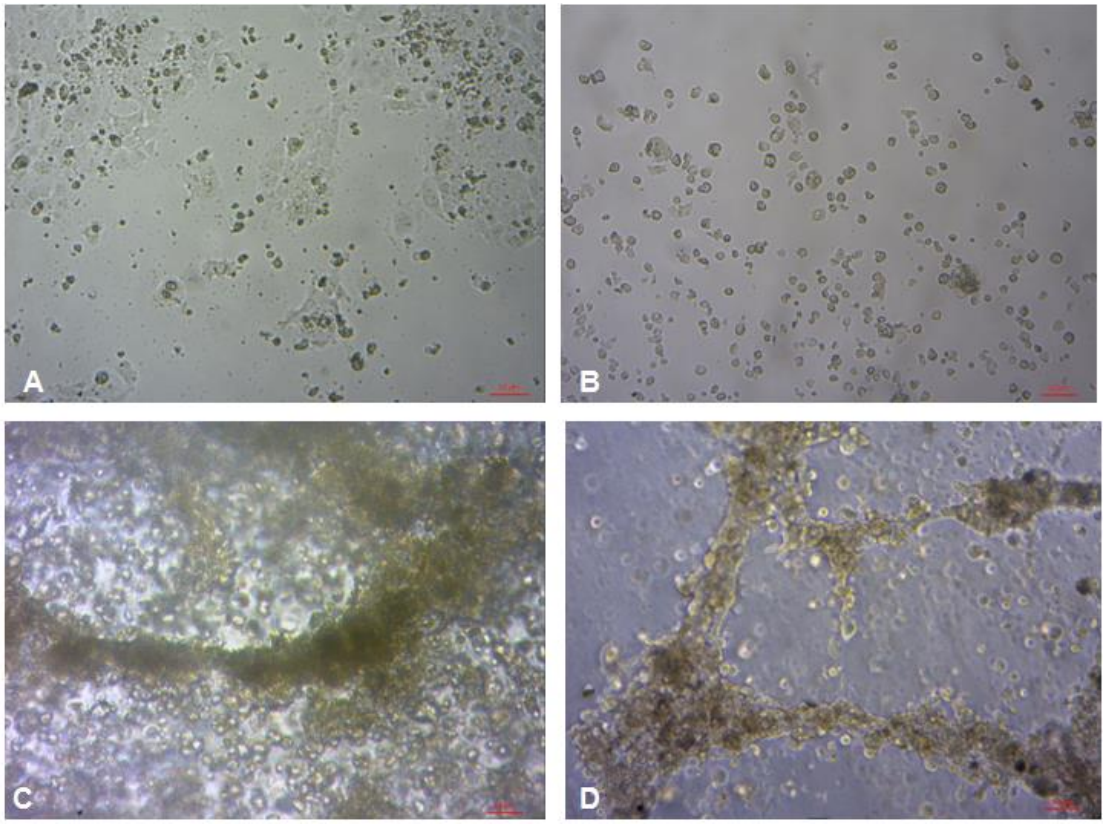

Figure 24: PC3 cell culture pre- and post-knockdown. Cultures were imaged at 10x magnification. A) 2D culture of PC3 cells; B) 2D culture of PC3 cells after PIP5K1A knockdown. No matrix formation is observed; C) 3D culture of PC3 cells co-cultured with endothelial cells in Matrigel®. Cells grow next to the endothelial cells, forming clusters with them; D) 3D culture of PC3 cells after PIP5K1A knockdown and co-culture with endothelial cells in Matrigel®. Cells grow as single cells without making junctions.

Clinical Cases

The three candidate genes (MYADM, PIP5K1A, and MYO1B) were tested with flow cytometry (immunostaining for extracellular as well as intracellular antigens) on clinical samples from patients with prostate cancer. Moreover, genes of patients with breast or colorectal cancer and genes of healthy individuals were also tested. The analysis revealed that there is no statistically significant difference among healthy and cancer cases (MYADM p=0.31, MYO1B p=0.17, PIP5K1A p=0.23). Data analysis is presented in **Table 9**, while selective flow cytometry graphs are presented in **Figures 25–28**.

Table 9: Expression of biomarkers (in %) after flow cytometry analysis. Positive values on negative controls indicate auto-fluorescence.

Sample	Control	MYADM	MYO1B	PIP5K1a
Healthy 1	0.06	0.21	0.29	0.36
Healthy 2	1.74	1.33	0.92	1.27
Healthy 3	0.14	0.34	0.31	0.46
Healthy 4	0.44	1.19	0.71	0.24
Healthy 5	0.14	0.99	0.74	1.2
Patient 1	0.04	1.57	0.56	7.57
Patient 2	0.07	0.41	0.07	0.58
Patient 3	0.05	0.11	0.06	0.96
Patient 4	0.09	1.31	0.09	0.21
Patient 5	0.18	0.81	0.09	11.2
Patient 6	0.11	0.21	0.08	0.29
Patient 7	0.22	1.27	0.04	0.4

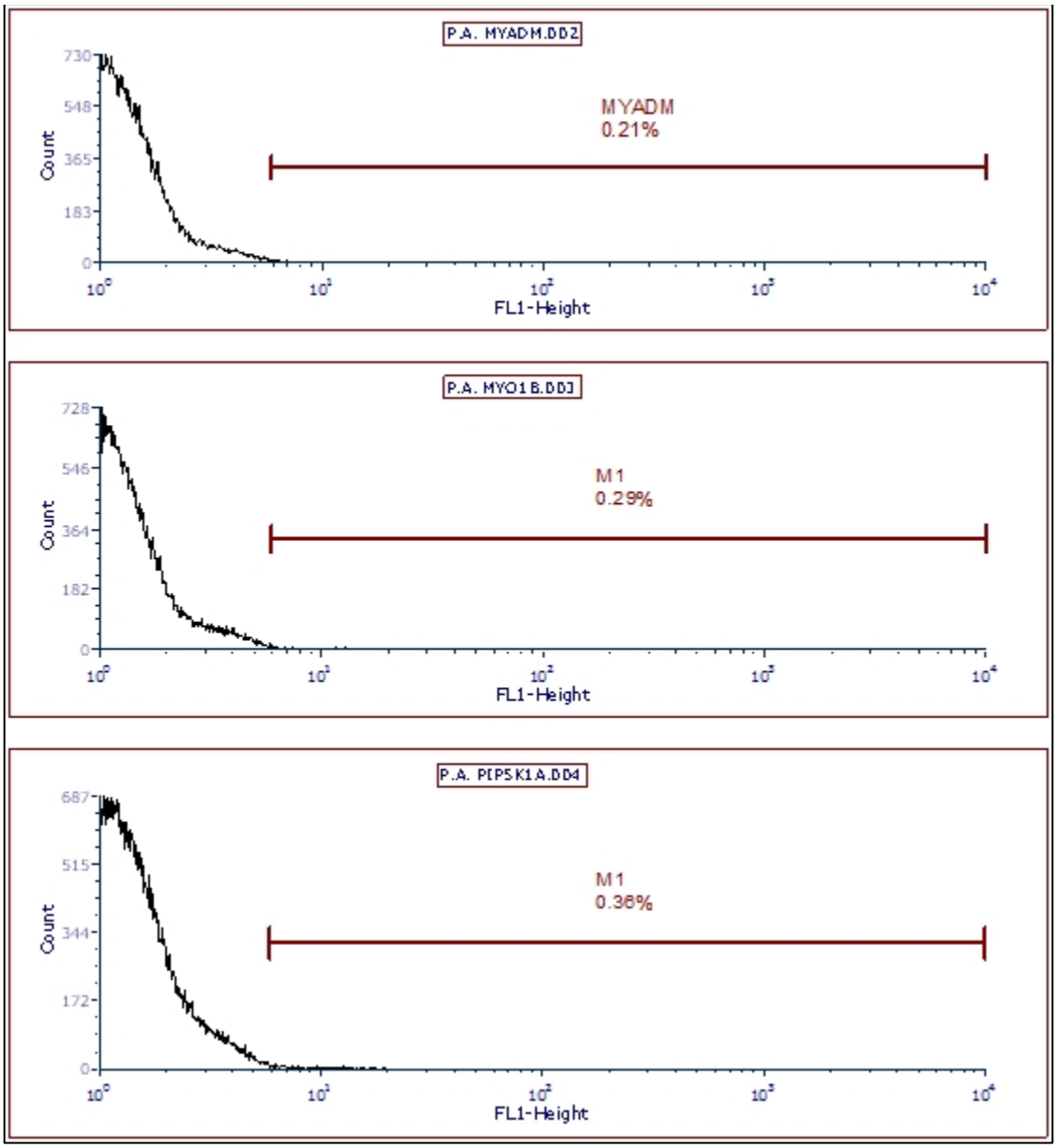

Figure 25: Flow cytometry histograms from healthy individual no. 1 for the three biomarkers.

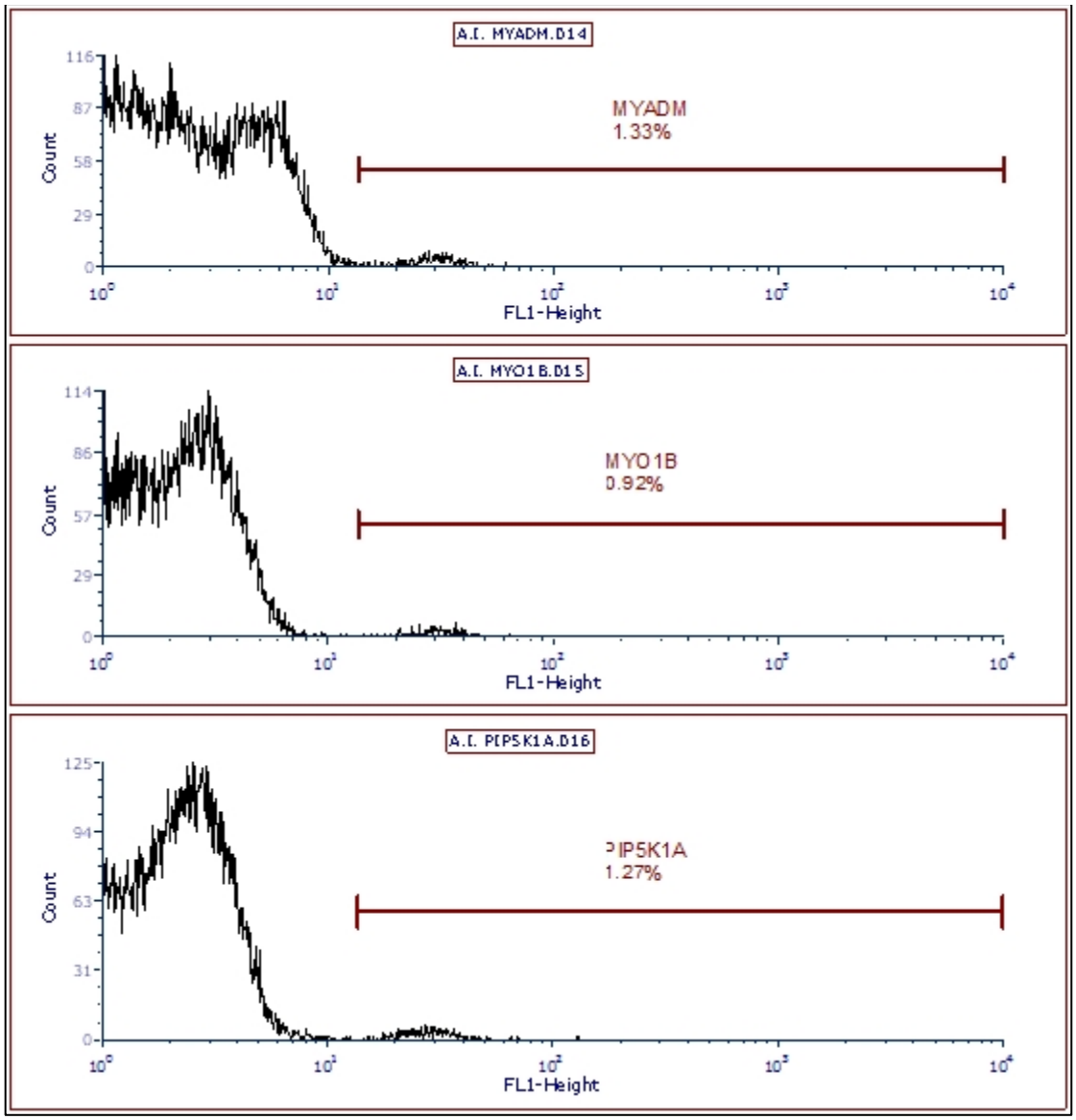

Figure 26: Flow cytometry histograms from healthy individual no. 2 for the three biomarkers.

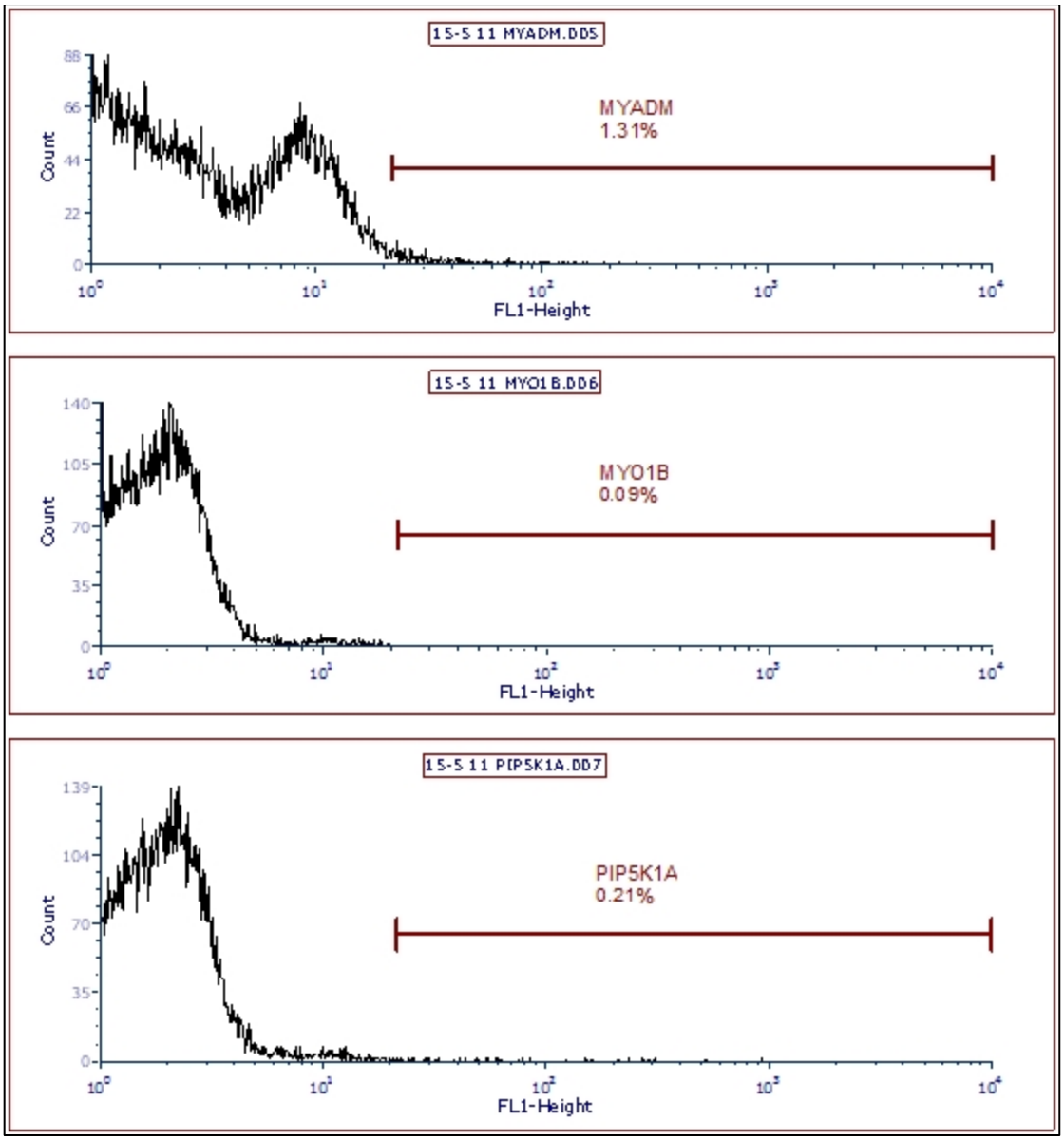

Figure 27: Flow cytometry histograms from cancer patient no. 1 for the three biomarkers.

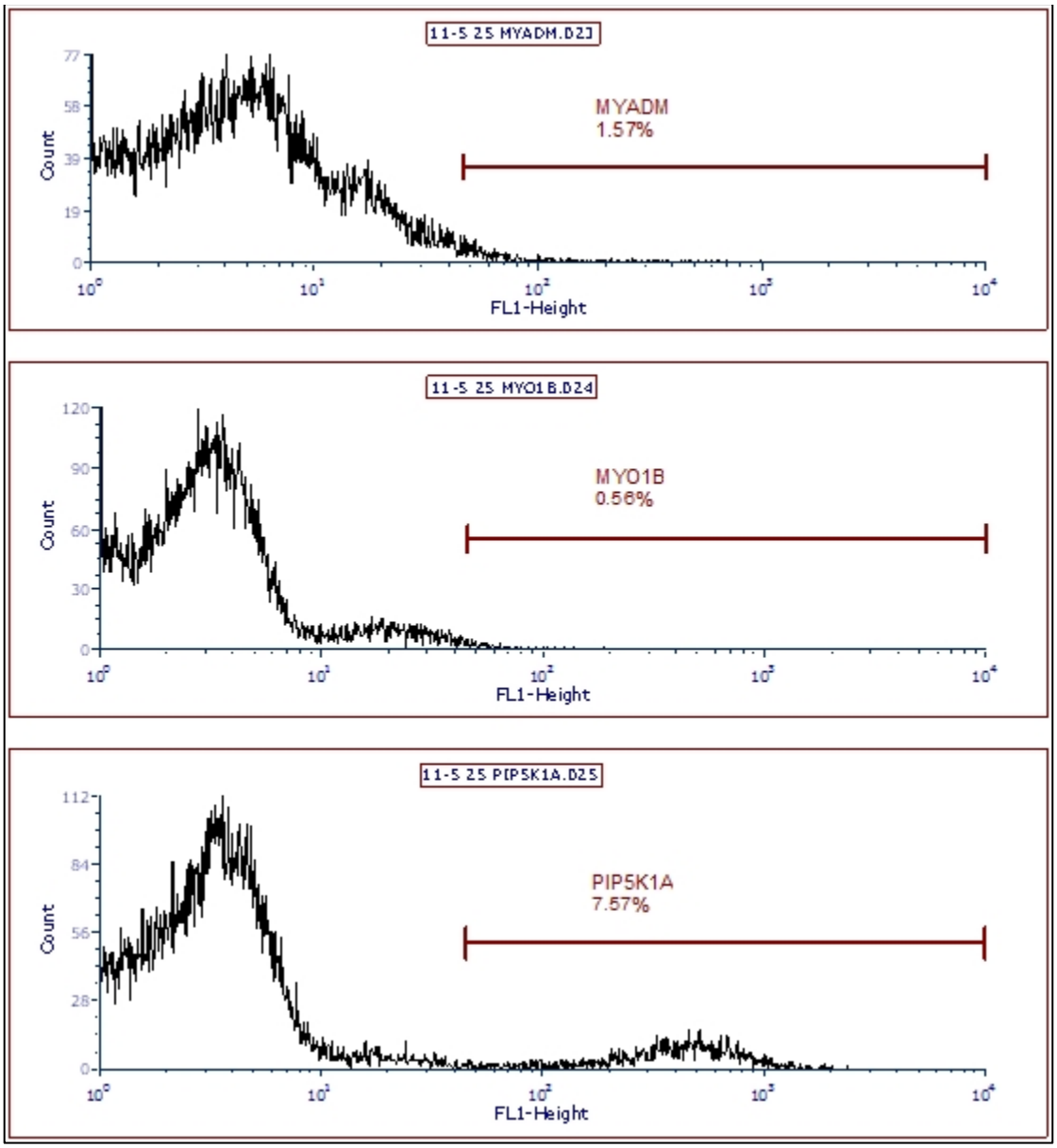

Figure 28: Flow cytometry histograms from cancer patient no. 1 for the three biomarkers.

Discussion

The detection of potential biomarkers expressed in prostate tumors would be beneficial for patients, as they could serve as indicators of lymph node metastasis. With the help of such biomarkers, physicians could distinguish metastasis to lymph nodes or to osteoblasts. During the surgery, the presence of markers associated with lymph node metastasis could be observed using rapid staining tests. Based on this, physicians could decide whether a lymphadenectomy should be performed or not.

Among the genes that were selected from microarrays experiments, those correlating with invasion, adhesion, and/or motility were selected for further analysis. The concept for further analysis was to identify a specific molecule that might be used as an indicator for lymph node metastasis. This biomarker should be expressed in prostate tumors and have a different expression on being co-cultivated with osteoblasts or endothelial cells, respectively. The molecules initially selected were SPAG9, FGF7, PIP5K1A, MYADM, PTGER4, OCLN, MYO1B, PRDM4, and KLK15. Only five of these were selected for further experiments, since they showed different expression patterns on co-cultivation with endothelial cells and osteoblasts, respectively. The cell lines where the molecules were successfully knocked down were submitted to a gene expression analysis of the genes correlated with invasion, motility, adhesion, metastasis, proliferation, and aggressiveness of cancer, in order to investigate the optimum results.

It was further found that the sperm-associated antigen 9 (SPAG9) is correlated with tumor development, cell proliferation, cell survival, and cell apoptosis. It is thought to contribute to prostate cell growth, possibly by regulating cyclin proteins (cyclin D1 and cyclin E).

SPAG9 is a scaffolding protein that brings MAPKs and their target transcription factors together to execute specific signaling pathways (Li et al. 2014). It belongs to the JNK-interacting protein family and takes part in molecular interactions during mitogen-activated protein kinase, signaling pathway and sperm-egg fusion. SPAG9 expression shares a close relationship with the Gleason score, NED rate, and radical prostatectomy. A high SPAG9 expression predicts a poor prognosis for prostate cancer patients (Sun et al. 2017).

Keratinocyte growth factor (KGF)/fibroblast growth factor-7 (FGF7) is a paracrine and epithelium-specific growth factor that regulates cell migration and invasion, and the paracrine sources of KGF/FGF7 are one of the malignancy-contributing factors from tumor stroma. KGF/FGF7 activates nuclear factor kB (NF-kB), which in turn activates VEGF, MMP9, and

urokinase-type plasminogen activator and enhances migration and invasion of epithelial cells (Niu et al. 2007). FGF7 may be responsible for the development of castration-resistant prostate cancer by enabling the survival of cells in the presence of a castrate environment. FGF7 activates the receptor tyrosine kinase FGFR2IIIb and this binding leads to FGFR2 dimerization. This in turn triggers RAS-mitogen-activated protein kinase (MAPK) and phosphoinositide 3-kinase (PI3K) AKT signaling pathways, which play an important role in tumor progression (Huang et al. 2017).

The lipid kinase phosphatidylinositol-4-phosphate 5-kinase type 1 alpha (PIP5K1A) regulates the PI3K/AKT/androgen receptor pathways and results in cancer cell proliferation, invasion, and survival. IP5K1A catalyzes the phosphorylation of phosphatidylinositol 4-phosphate (PtdIns4P) to form phosphatidylinositol 4,5-bisphosphate (PtdIns(4,5)P2). In the nucleus, PIP5K1A interacts with Star-PAP (nuclear speckle targeted PIPKIalpha regulated-poly(A) polymerase) through PtdIns(4,5)P2, regulating its activity and therefore gene expression (Mellman et al. 2008). Star-PAP polyadenylates select a subset of mRNAs in the cell involved in oxidative stress response, apoptosis, and cancer and exhibit a tumor-suppressing activity in breast cancer (Yu et al. 2017). Apart from production of (PtdIns(4,5)P2), PIP5K1A is an upstream regulator of Rac1, which in turn is involved in the control of actin dynamics and cell migration (Chao et al. 2010). PIP5K1A produces PIP2, which is required for PI3K/AKT activation. Overexpression of PIP5K1A is associated with poor prognosis in prostate cancer and is related to elevated levels of the androgen receptor (Semenas et al. 2014). Metastatic lesions contain significantly higher levels of PIP5K1A and AR compared with primary tumors. It increases the expression of AR, which forms protein-protein complexes in the nucleus with the cell cycle protein CDK1 (Flemming 2014).

The myeloid-associated differentiation marker (MYADM) is involved in the organization of membranes for cell migration. It colocalizes with Rac1 in membrane protrusions at the cell surface and distributes in condensed membranes. MYADM and Rac1 act on parallel pathways that lead to similar functional outcomes. MYADM plays an important role in lamellipodium extension and in cell motility (Aranda et al. 2011).

Rac1 is a Rho-family guanosine triphosphatase (GTPase) that regulates the spreading and actin-mediated extension of lamellipodia (Ridley et al. 2003). MYADM also regulates the proteins ezrin, radixin, and moesin (ERM), which are connectors between the plasma membrane and the cytoskeleton and regulate the structure and function of filopodia,

therefore signaling processes such as motility and cytokinesis (Fehon et al. 2010). The ERM expression in turn regulates the expression of the intercellular adhesion molecule (ICAM)-1 (Clark et al. 2007; Aranda et al. 2013). It is also noteworthy that upon activation of ERM, a specific domain (N-terminal four point one, ezrin, radixin-moesin [FERM]) interacts with PtdIns(4,5)P2, whose role was explained above (Kwiatkowska 2010). As mentioned, PtdIns(4,5)P2 regulates the activity of Star-PAP poly(A) polymerase, which in turn might regulate the expression of different mRNAs associated with cell protection (Mellman et al. 2008).

The SSX2IP gene encodes a protein that binds the cancer-testis antigen Synovial Sarcoma X breakpoint 2 protein. The encoded protein may regulate the activity of Synovial Sarcoma X breakpoint 2 protein in malignant cells. Alternate splicing results in multiple transcript variants. A pseudogene of this gene is found on chromosome 3. It belongs to an adhesion system that plays a role in the organization of homotypic, interneuronal, and heterotypic cell-cell adherens junctions (AJs). It may connect the nectin-afadin and E-cadherin-catenin system through alpha-actinin and may be involved in the organization of the actin cytoskeleton at AJs through afadin and alpha-actinin. It is also involved in cell movement. Thus, it is localized at the leading edge of moving cells in response to PDGF and is required for the formation of the leading edge and the promotion of cell movement, possibly via activation of Rac signaling. It acts as a centrosome maturation factor, probably by maintaining the integrity of the pericentriolar material and proper microtubule nucleation at mitotic spindle poles. The function seems to implicate WRAP73 at least in part; it is suggested that the SSX2IP:WRAP73 complex acts as a regulator of spindle anchoring at the mitotic centrosome. Moreover, it is involved in ciliogenesis, being required for targeted recruitment of the BBSome, CEP290, RAB8, and SSTR3 to the cilia. The expression of SSX proteins in tumor tissues has been associated with advanced stages of disease and worse patient prognosis (Smith and McNeel 2010).

The PTGER4 encodes a receptor for prostaglandin E2 (PGE2). The activity of this receptor is mediated by G(s) proteins that stimulate adenylate cyclase. It has a relaxing effect on smooth muscles and may play an important role in regulating renal hemodynamics, intestinal epithelial transport, adrenal aldosterone secretion, and uterine function. PTGER4 is a protein-coding gene. Diseases associated with PTGER4 include malignant epithelial mesothelioma and epididymis cancer. Among its related pathways are eicosanoid ligand-binding

receptors and signaling by GPCR. The protein encoded by this gene is a member of the G-protein-coupled receptor family. This protein is one of four receptors identified for prostaglandin E2 (PGE2). This receptor can activate T-cell factor signaling. It has been shown to mediate PGE2-induced expression of early growth response 1 (EGR1), to regulate the level and stability of cyclooxygenase-2 mRNA, and to lead to the phosphorylation of glycogen synthase kinase-3. Knockout studies in mice suggest that this receptor may be involved in the neonatal adaptation of the circulatory system, in osteoporosis, as well as in the initiation of skin immune responses. The blockage of PGE2-EP4 signaling prevents the bone destruction required for prostate metastases and this is in part due to the abrogation of bone cell responses. The EP4 antagonist is a candidate for the treatment of prostate cancer in the blockage of bone metastases (Watanabe et al. 2016).

OCLN (Occludin) is a protein-coding gene. Diseases associated with OCLN include Pseudo-Torch Syndrome 1 and Torch Syndrome. Among its related pathways are Development Slit-Robo signaling and Blood–Brain Barrier and Immune Cell Transmigration: VCAM-1/CD106 Signaling Pathways. This gene encodes an integral membrane protein required for cytokine-induced regulation of the tight junction paracellular permeability barrier. Mutations in this gene are thought to be a cause of band-like calcification with simplified gyration and polymicrogyria (BLC-PMG), an autosomal recessive neurologic disorder also known as pseudo-TORCH syndrome. A related pseudogene is located 1.5 Mb downstream on the q arm of chromosome 5. It may play a role in the formation and regulation of the tight junction (TJ) paracellular permeability barrier. It is able to induce adhesion when expressed in cells lacking tight junctions. Occludin is expressed in all stages of prostate cancer (Furuse et al. 1993; Ekinci et al. 2020; Jędroszka et al., 2017).

Myosin 1b (MYO1B) is a member of the myosin superfamily proteins and involved in organelles transportation, membrane tension generation, and muscle contraction (Heissler and Sellers 2016). In prostate cancer cell lines, MYO1B is expressed in high levels in cells with high metastatic potential. It can directly influence actin organization and cell morphology that can contribute to the metastatic phenotype. Expression levels of MYO1B are significantly higher in PC3 than in LNCaP cells. High endogenous levels of MYO1B in more highly metastatic cells might increase cortical tension, allowing cells to move through stiff extracellular matrices *in vivo*, which explains why knockdown of MYO1B only affects migration in 3D but not 2D

(Makowska et al. 2015). MYO1B correlates with proliferation, migration, and invasion in other types of cancer (Zhang et al. 2018; Ohmura et al. 2015) and contributes to membrane trafficking by controlling the shape of organelles (Yamada et al. 2014). MYO1B might be involved in migration by participating in filopodia and lamellipodia formation as well as by regulating actin assembly (Diz-Muñoz et al. 2010; Almeida et al. 2011). The localization of MYO1B within filopodia requires MYO1B to bind with phosphoinositides, indicating once again their role in migration (Komaba and Coluccio 2010).

PR/SET domain 4 (PRDM4) is a transcription factor interacting with YAP WW domains. It cooperates with TEAD to mediate YAP-induced ITGB2 expression. ITGB2 and PRDM4 are significantly higher in metastatic prostate cancer than in normal tissue or clinically localized cancer. Activation of YAP and PRDM4 may contribute to elevated ITGB2 expression in metastatic prostate cancer (Liu, Shangli et al. 2018; Liu, Dai et al. 2018; Liu, Liang et al. 2018).

Kallikrein-related peptidase 15 (KLK15) expression levels are upregulated in CaP compared to benign prostate tissues and in advanced disease. KLK15 is also associated with advanced pathological stages. It is located adjacent to KLK3 on chromosome 19q13.4, which is a prostate specific antigen (Yousef et al. 2002).

CD44 is a transmembrane glycoprotein involved in cell–cell and cell–matrix adhesion. The abnormal expression is correlated with different types of cancer including prostate carcinoma. It has been proved that the expression of CD44 is downregulated in prostate tumors (De Marzo et al. 1998). However, it has a functional role in invasion (Omara-Opyene et al. 2004). The role of SNAI1 in EMT (epithelial-mesenchymal transition) is well-studied, through downregulation of cell adhesion molecules (Cano et al. 2000). In addition, the knockdown inhibits the invasiveness, revealing SNAI1's role in the aggressiveness of prostate cancer (Deep et al. 2014). Integrin αV (ITGAV) has been implicated in prostate cancer progression and mAb are used against integrins αV impacts (Jiang et al. 2017). Furthermore, ITGAV is correlated not only with prostate cancer maintenance, but also with bone metastasis (van der Horst et al. 2011). KRT19 is studied as a biomarker for prostate cancer, including also other serum proteins such as FLNA and FLNB (Ravipaty et al. 2017). The Twist1 transcription factor is a regulator in the epithelial-to-mesenchymal transition and has been proved to be implicated in prostate cancer metastasis (Gajula et al. 2013). Vimentin is also involved in invasiveness of prostate

cancer, through src regulation (Wei et al. 2008). Apart from invasiveness, it also affects the prostate cancer cells' motility (Zhao et al. 2008).

Beta-catenin is correlated with adhesion and signal transduction and a lot of mutations have been observed in prostate cancer (Voeller et al. 1998), while overexpression can promote invasive prostate cancer (Francis et al. 2013). In prostate cancer, CDH1 (E-cadherin) abundance and activity are inversely associated with cell invasiveness and motility (Keil et al. 2014). N-cadherin (CDH2) is implicated in EMT and has been demonstrated to be overexpressed in tumor cells from different types of cancer (Wheelock et al. 2008). DPP4 encodes a membrane-anchored protein that cleaves dipeptides from multiple growth factors, resulting in their increased degradation. The inhibition of DPP4 with sitagliptin enhanced the growth of prostate cancer xenografts following castration. Significantly, DPP4 inhibitors are frequently used to treat type 2 diabetes, as they increase insulin secretion. Together, these results point to DPP4 as an AR-regulated tumor suppressor gene whose loss enhances growth factor activity and suggest that treatment with DPP4 inhibitors may accelerate the emergence of resistance to ADT (Russo et al. 2018). The decreased expression of DSC1 molecules facilitates metastatic and aggressive tumor behavior and a poorer prognosis in squamous carcinomas and cell lines (Myklebust et al. 2012). PTK2 is part of the FAK family. The SRC/FAK pathway is associated with spinal metastasis of prostate cancer cells and is regulated by the expression levels of CXCL1/CXCR1. CX3CL1/fractalkine enhances prostate cancer spinal metastasis by activating the Src/FAK pathway. ITGA5 is a migration-related gene and plays an important role in mediating cell adhesion and migration in cancer. The expression of ITGA5 can increase the formation of mother vessels by stimulating the VEGF-A pathway. The downregulation of ITGA5 prevents all steps of metastasis. Caveolin 2 (CAV2) is a cell membrane protein involved in cancer progression. The downregulation of CAV2 inhibits proliferation, migration, and invasion (Liu, Shangli et al. 2018; Liu, Dai et al. 2018; Liu, Liang et al. 2018; Kamibeppu et al. 2018). SNAI2 is a zinc finger protein playing an essential role in the proliferation and invasiveness of prostate cancer, while also affecting cytoskeleton and adhesion. The downregulation leads to the inhibition of invasion and disturbed microtubule and actin cytoskeletons (Emadi Baygi et al. 2010). Moreover, it has been proved that SNAI2 promotes migration and invasion through the suppression of CDH1 (Peinado et al. 2007). EGFR overexpression has been implicated in survival of tumor-initiating cells, circulating tumor cells, and metastasis to the bones (Day et

al. 2017). CLDN3 is overexpressed in many types of cancer including ovarian, pancreatic, breast, and prostate cancers. It regulates motility and invasion through the Wnt pathway. In hepatocellular carcinoma, it inhibits cancer invasiveness and tumor formation (Jiang et al. 2014; Morin 2005). ITGB1 is a molecule involved in cell adhesion and metastasis, while in prostate cancer it is involved in TGFβ signaling and contributes to the switch from suppressive to oncogenic (Pellinen et al. 2018). IGF1R is involved in prostate cancer and particularly enhanced in tumor growth, migration, and angiogenesis (Heidegger et al. 2014). The epithelial-mesenchymal transition (EMT) is a process by which epithelial cells lose their cell polarity and cell–cell adhesion and gain migratory and invasive properties to become mesenchymal cells. Apart from numerous developmental processes, EMT is important for the initiation of metastasis. The mesenchymal-epithelial transition (MET) is the opposite process essential for the creation of new metastatic sites. The adhesion and invasive features of cells are important for the complete process of metastasis (Lee et al. 2006).

Taking everything into consideration and also studying the signal transduction pathways of the above genes (see Raw Data section), some of the molecules might be used as indicators of metastasis to lymph nodes.

The Matrigel® co-cultivation of cancer cells with endothelial cells enabled interactions that would otherwise be difficult or impossible in two-dimensional cultures. In general, the knocked-down cells demonstrated a slightly different phenotype (smaller-sized cells than the controls). Moreover, in contrast to the control cells, some cell lines such as VCaP showed a reduced ability to form clusters while in 3D culture. A complete formation of vascular structures was not observed in most of the cultures. However, this may be due to the fact that cultures were broken down for RNA extraction on the 4th day. 2D cultures of knocked-down cell lines demonstrated an inability to adhere to the surface, hence they grew in suspension. This may stem from the fact that the knocked-down genes were associated with genes that regulate cell adhesion and migration.

The KD of MYADM caused the decrease of ITGB1, IGF1R, and TWIST1 in all cell lines, sensitive as well as insensitive ones. Distinct patterns were observed for FN1, ITGA5, ITGAV, and PECAM1, where upregulation was observed in refractory cell lines, but downregulation in sensitive ones. Stable KD of MYO1B led to the downregulation of ITGB1 and IGF1R in all cell lines

tested, while CTNNB1 and DSC1 upregulated. The overexpression observed for MET and PECAM1 applied only to insensitive cell lines. The downregulation of ITGB1 and IGF1R was also identified post PIP5K1A KD, but no other pattern was observed among the other molecules. The study of signal transduction pathways showed cross-talking for most of these genes. This could explain the non-expected expression patterns in some of the associated genes (see Raw Data section under “pathways”).

The flow cytometric analysis of clinical and healthy samples did not reveal any statistically significant difference. However, certain samples showed a higher expression of PIP5K1a in comparison to all others. Further information about those samples is required in order to draw safer conclusions. Also, the testing was done on blood samples and not on tissues, which is why there might be a difference in the expression of those markers depending on the origin of the sample.

Thus, MYADM, PIPSK1A, and MYO1B in primary prostate cancer tumors could indicate future lymph node metastasis and could help guide lymph node dissection in prostate cancer patients.

The dissection of lymph nodes is based mainly on D’Amicos risk classification for prostate cancer, which is associated with the levels of Prostate Specific Antigen (PSA), the Gleason score, and the clinical stage (D’Amico et al. 1998). However, the value of pelvic lymph node dissection in patients with prostate cancer, based on D’Amico’s classification risk, remains unclear (Preisser et al. 2020). Apart from this, other classification systems for managing prostate cancer treatment have been proposed, such as the ‘Candiolo’ classifier (Gabriele et al. 2016). Based on our experimental data – which of course need to be validated with clinical samples – the study of at least one of the three markers (MYADM, MYO1B, PIP5K1A) on the tumor (e.g. by histological techniques) contributes to a rapid classification system independent from hormone sensitivity.

Conclusion

The detection of markers able to predict the metastasis to lymph nodes might be helpful in the management of prostate cancer, as the removal of lymph nodes could be beneficial for the patient. The present study identified a number of biomarkers that are expressed in

prostate cancer, but whose expressions differed depending on whether the prostate cancer cells were co-cultivated with osteoblasts or with endothelial cells. These genes were also involved in procedures required for metastasis, and their knockdown altered the expression of key regulators for EMT, invasion, motility, and migration. Therefore, the detection of MYADM, PIP5K1A, or MYO1B in a primary tumor could be used as an indicator for future metastasis in lymph nodes. To prove this concept, the examination of more tissue samples would be required.

Abstract

Background: Prostate cancer is the most frequent type of cancer among men worldwide. The treatment protocol depends on the extension of the disease and on whether the carcinoma is hormone-refractory or hormone-sensitive. Hormone-refractory carcinoma exhibit a different protein profile at the surface as well as different migration abilities and interactions with organs and tissues than hormone-sensitive carcinoma. Prostate cancer most commonly metastasizes to the bones and lymph nodes, and after local progression it may invade the rectum, bladder, and lower ureters. Surgical excision of inguinal or other regional lymph nodes is recommended and beneficial for patients as it prevents metastasis through the lymph nodes. However, not all cases metastasize through the regional lymph nodes. Therefore, the present study analyzed different human prostate carcinoma cell lines grown in a 3D culture model environment resembling the environment of bone or lymph node niches. The aim of the study was to detect niche specific biomarkers that predict whether the metastasis will proceed through the lymph nodes or metastasize via the hematogenic route to the bones or other organs.

Materials & Methods: Two categories of human prostate carcinoma cell lines were selected: one group of hormone-sensitive cell lines and one group of hormone-refractory cell lines that had developed bone metastases. The first group consisted of the three sensitive cell lines LNCap, VCaP and MDA-PCa-2b, while the hormone-insensitive group consisted of the cell lines PC-3, DU 145 and SerBob. The cancer cell lines were grown in a 3D culture model resembling the bone or lymph node micro-environment. The bones environment was developed on a co-cultivation model between Human Osteoblasts (HOb) and the relevant prostate cancer cell line. The lymph nodes micro-environment was similarly developed on a co-cultivation model between the endothelial cell line (HDLEC) and the relevant prostate cancer cell line. 3D cell cultures were grown with Matrigel®, which resembles the extracellular environment found in many tissues and is used as a substrate for culturing cells. RNA was isolated from the co-cultures and whole gene expression microarray experiments followed. Targets expressed in prostate cancer whose expression alters upon metastasis to lymph nodes in a different way than in bone metastasis were further studied. These targets were knocked down on the cancer cell lines, which was followed by a repetition of co-cultivation experiments with HDLEC. Gene expression assays were then done in order to validate the implication of the new potential biomarkers in metastasis.

Results: As expected, the two groups of cell lines expressed different levels of prostate-specific membrane antigen. The co-culture experiments in a 3D environment revealed hundreds of differentially-expressed genes when co-cultivated with osteoblasts or endothelial cells. We also compared gene expression between co-cultivated cells, osteoblasts, endothelial cells, and cancer cell lines. Genes highly

expressed before co-cultivation were not included in the final analysis. Therefore, the differentially-expressed genes MYADM, PIP5K1A, PTGER4, MYO1B, SPAG9, OCLN, PRDM4, SSX2IP, KLK15, and FGF7 were selected for further depletion knockdown experiments. All of the above markers were expressed in the initial cancer cell lines and changed their expression after co-culture. Finally, the genes MYADM, PIP5K1A, and MYO1B were selected, since their expression increased upon cultivation with endothelial cells, while when co-cultured with osteoblasts, the expression decreased in the majority of the cell lines. The knockdown of the above genes led to alterations in the expression of gene levels essential for metastasis, including integrins and growth factor receptors, amongst others. In particular, MYADM knockdown caused a decrease in ITGB1, IGF1R, and TWIST1 expression in all cell lines, whereas FN1, ITGA5, ITGAV, and PECAM1 were upregulated in hormone-refractory cell lines and downregulated in hormone-sensitive cells. MYO1B knockdown decreased ITGB1 and IGF1R expression levels and upregulated CTNNB1 and DSC1 in all tested cell lines. Furthermore, we observed that MET and PECAM1 were overexpressed in hormone-sensitive cell lines. Finally, integrin receptors ITGB1 and IGF1R were downregulated after PIP5K1A knockdown in all tested cell lines.

Discussion: Biomarkers associated with prostate cancer metastasis to lymph nodes would be helpful for prostate cancer management, since in these incidences, the removal of lymph nodes could be beneficial for the patient. Up to now, the dissection of lymph nodes is generally based on D'Amico's risk classification for prostate cancer, which is associated with the levels of Prostate Specific Antigen (PSA), the Gleason score, and the clinical stage. The predictive value of this algorithm is unclear since it is very difficult to stratify prostate cancer patients who will gain a clinical benefit from the regional and/or inguinal lymph node clearance from those who will not. Therefore, a model based on a few niche specific biomarkers, using easy-to-perform and well-established techniques, is lacking and very much required. MYADM, MYO1B, and PIP5K1A constitute three biomarkers that are detected in primary hormone-refractory or hormone-sensitive prostate tumors and can predict the metastasis of the primary tumor to regional (iliac) lymph nodes. The detection of these biomarkers can be easily performed using histological methods or nanopore technology. This enables a quick decision about lymph nodes clearance, even during the operation procedure. For use at the clinical level, the above markers still need to be validated on clinical samples.

Raw Data

DNA microarrays

Table 10: Insensitive: markers expressed in co-cultivation with osteoblasts.

Gene Name	Function
COL11A1	Skeletal morphogenesis, fibrillogenesis
COMP	Pathogenesis of osteoarthritis, human limb development, protects cells against death
GREM1	Early limb outgrowth, inhibits growth or viability of normal cells, inhibits differentiation of osteoblasts.
LEP	Regulates bone mass and secretion of hormones, pro-angiogenic for endothelial cells, affects innate and adaptive immunity.
SSH1	Actin dynamics
TAGLN	Replicative senescence, senescent human fibroblasts

Table 11: Insensitive: markers expressed in co-cultivation with endothelial cells.

Gene Name	Function
TMEM209	Cell growth
PELO	Chromosome segregation
RAB18	Apical endocytosis/recycling, eye and brain development, neurodegeneration
RCBTB1	Cell cycle regulation
SCAMP1	Cell surface recycling
SLC25A24	Buffering calcium levels in the mitochondrial matrix
TIFA	Immune response
NEDD1	Mitosis progression

Table 12: Sensitive: markjkkkers expressed in co-cultivation with osteoblasts.

Gene Name	Function
PEX7	Peroxisomal biogenesis – synthesis of lipids
PDGFRB	Growth factor receptor
ITGBL1	EGF-like protein family
HAS1	Hyaluronan synthesis
RB1CC1	Interacts with signaling pathways to coordinately regulate cell growth, cell proliferation, apoptosis, autophagy, and cell migration. This tumor suppressor also enhances retinoblastoma 1 gene expression in cancer cells.
GREM1	Cytokine, BMP (bone morphogenic protein)-antagonist family, inhibits BMP2-mediated differentiation of osteoblasts.
FOSB	AP-1 transcription factor subunit
EYA2	Eye development
LTBP2	Growth factor beta binding protein
FMOD	Assembly of the collagen fibers of the extracellular matrix
RRAD	Regulates voltage-dependent L-type calcium channel subunit alpha-1C trafficking to the cell membrane.
COX7A1	Cytochrome c oxidase
CCDC80	Cell adhesion and matrix assembly. Downregulated in cancer and after osteoblastic differentiation.
COMP	Structural integrity of cartilage. Potent suppressor of apoptosis.
MYADM	Expressed in myeloid cells, upregulated during differentiation of stem cells and myeloid leukemia cells.
HOOK1	Cytoskeleton, microtubules
ADAMTS2	Collagen biosynthesis
PPFIBP1	Axon guidance and mammary gland development
COL1A1	Collagen biosynthesis
COL3A1	Collagen biosynthesis

COL8A1	Component of the basement membrane of the corneal endothelium.
COL11A1	Minor fibrillar collagen

Table 13: Sensitive: markers expressed in co-cultivation with endothelial cells.

Gene Name	**Function**
CDC123, CDK1, CCNG1, PKN2, AHR, EPS15, IK, ILKAP, CCNB1IP1, CTDP1, PDS5B, PSMC4, PSMD13, SLBP	Cell cycle regulation
DUX4, HIF1A, MATR3, MED1, AC027125.1, ACTN4, AHR, DAPK3, DHX9, EWSR1, IK, IKZF5, ZNF160, ZNF253, ZNF28, ZNF33B, ZNF12, ZNF346, ZNF654, ZNF790, ZNF93, ZBTB33, ZBTB44, ZHX1, CTBP2, PAPOLA, RPP38, SERBP1, SIRT2, SMN1, SUPT4H1, TBPL1	Transcription/Post-transcription regulator
ASAH1, ASPH, C11orf31, ASNS, GOT2, ISOC2, MGST3, MMADHC, MGAT4B, CYP20A1, FECH, ACADM, ALG3, ATP6V0D1, ATP6V1D, ATP7A, COQ10B, GFPT1, MB, MTMR2, PNPLA8, PRPS2, PRPSAP2, TMX2, UGT2B17, WBSCR22, TM9SF2	Metabolism
ATG4A, C9orf72, SCOC, TRIM5	Autophagy
CDK10, AC008810.1, ADD1, C6orf168, DAPK3, LARP4, IFT81, LMNB1, LMAN1, HDAC2, RABGAP1, SAP30, SMEK2, TFG, SEPT2, PAFAH1B1	Cytoskeleton
EIF5, EIF2AK3, EIF4A2, GANAB, DAPK3, LARP4, NXT2, CNOT6, KIAA1429, KLHL8, WSB1, COMMD10, FBXO3, FURIN, LGMN, NMD3, NOL11, RFWD2, RNF11, RNF181, USP10, P4HA1	Translation/Post-translation regulator
DSG2, PKN2, ILKAP, ENAH, VAPA, RAC3	Cell adhesion
DDB2, RAD50, PSMC4, PSMD13, RNF138, SHPRH, TDG	Repair mechanism

BIRC1, CASP6, ANKHD1, DAPK3, MOBKL1A, DNAJA1, PSMC4, PSMD13, TAX1BP1, TM7SF3, TRIAP1	Apoptosis/Cell death
AC008810.1, EPS15, ZNF3, CNOT6, MOBKL1A, PIK3C2A, USP8, WNK1	Cell proliferation
PKN2, MOBKL1A, VEGFA	Cell migration
C6orf170, DUSP3, JKAMP, KCTD6, TTC3, WNK1	Signaling
DHX9, FAF1, RBBP6, XRCC6	Replication
ERP29, HKE2, HERPUD2, BAG5, TMX2	Protein folding
HP1BP3	Self-renewal
CBARA1, ETFA, MRPL40, UQCRC2, PPA2	Mitochondrial related
GOSR1, SCP2, RHOBTB3, DCTN6, SAMD8, SLC30A5, TRAPPC8, SCFD1, SULT1A1, TMED10, TOMM20, USO1, VPS13A, C20orf30	Peptide/protein etc. transporation
LRPAP1, NAP1L4,	Chaperone
ATP6V1E1, DNAJA2, TCP1, SMARCA5, PPFIA1, SUCLG1, UBXN6	ATP-related
FAM111B	Cancer-associated nucleoprotein
KIAA1598	Neuronal polarization and neurite outgrowth
KIAA1715	Endoplasmic reticulum morphology
LDHC	Sperm motility
PEX11A	Peroxisomal proliferation
SHANK2	Adapter protein in PSD of excitatory synapses

Transient Knockdown Experiments

Table 14: MYADM KD gene expression data. Relative quantification according to non-transfected cell line.

	DU145	PC3	SERBOB	MDA-Pca-2b
ACTB	0.00	0.00	0.00	0.00
CAV2	-0.22	-0.14	0.10	#VALUE!
CD44	-0.27	-0.04	-0.06	-0.12
CDH1	-0.17	0.04	0.07	0.13
CDH2	#VALUE!	-0.14	0.02	#VALUE!
CLDN3	-0.08	-0.06	0.25	-0.08
COL11A1	#VALUE!	#VALUE!	#VALUE!	#VALUE!
CTNNB1	-0.19	-0.05	0.17	0.07
DPP4	0.11	0.04	0.18	-0.01
DSC1	#VALUE!	0.26	0.27	1.48
EGFR	0.13	0.00	-0.12	0.26
EPCAM	#VALUE!	#VALUE!	#VALUE!	#VALUE!
FN1	-0.09	0.05	0.33	0.14
IGF1R	-0.15	0.00	0.12	-0.12
ITGA4	#VALUE!	-0.01	-0.09	#VALUE!
ITGA5	0.07	0.13	0.22	0.32
ITGA8	#VALUE!	#VALUE!	#VALUE!	-0.41
ITGAL	#VALUE!	#VALUE!	#VALUE!	#VALUE!
ITGAM	0.09	#VALUE!	#VALUE!	#VALUE!
ITGAV	0.01	0.06	0.19	0.10
ITGB1	-0.13	0.05	0.09	0.11
ITGB2	-0.12	-0.01	#VALUE!	0.04
ITGB3	-0.26	#VALUE!	#VALUE!	#VALUE!
KRT19	-0.11	-0.16	#VALUE!	-0.13
MET	-0.19	0.04	0.20	0.49
PECAM1	#VALUE!	-0.20	#VALUE!	#VALUE!
PTK2	0.07	0.01	0.06	0.16
SNAI1	-0.13	-0.02	-0.11	#VALUE!
SNAI2	-0.10	0.03	0.01	#VALUE!
TWIST1	#VALUE!	-0.40	0.20	-0.10
VASP	-0.14	0.20	0.12	0.34
VIM	-0.09	-0.29	0.05	#VALUE!

Table 15: PIP5K1A KD gene expression data. Relative quantification according to non-transfected cell line.

	DU145	PC3	SERBOB	MDA-Pca-2b
ACTB	0.00	0.00	0.00	0.00
CAV2	-0.23	-0.01	0.01	#VALUE!
CD44	-0.26	0.06	0.03	0.17
CDH1	-0.18	0.00	-0.11	0.07
CDH2	#VALUE!	-0.01	-0.03	#VALUE!
CLDN3	-0.11	-0.01	0.11	-0.01
COL11A1	#VALUE!	#VALUE!	#VALUE!	#VALUE!
CTNNB1	-0.17	0.00	0.05	0.13
DPP4	0.08	0.22	-0.05	0.02
DSC1	#VALUE!	0.25	-0.05	1.76
EGFR	0.07	-0.08	-0.01	0.47
EPCAM	#VALUE!	#VALUE!	#VALUE!	#VALUE!
FN1	-0.05	0.09	0.03	0.15
IGF1R	-0.20	0.05	-0.02	-0.06
ITGA4	#VALUE!	0.15	0.13	#VALUE!
ITGA5	-0.18	0.18	-0.01	0.02
ITGA8	#VALUE!	#VALUE!	#VALUE!	0.02
ITGAL	#VALUE!	#VALUE!	#VALUE!	#VALUE!
ITGAM	0.12	#VALUE!	#VALUE!	#VALUE!
ITGAV	-0.06	0.08	0.00	0.19
ITGB1	-0.24	0.13	-0.17	0.03
ITGB2	-0.23	0.14	#VALUE!	-0.23
ITGB3	-0.19	#VALUE!	#VALUE!	#VALUE!
KRT19	-0.16	0.14	#VALUE!	0.00
MET	-0.26	0.13	-0.02	-0.37
PECAM1	#VALUE!	0.19	#VALUE!	#VALUE!
PTK2	-0.05	0.24	-0.04	0.09
SNAI1	-0.11	0.15	0.14	#VALUE!
SNAI2	-0.20	0.31	-0.12	#VALUE!
TWIST1	#VALUE!	-0.26	-0.16	0.15
VASP	-0.27	0.35	-0.04	0.19
VIM	-0.11	0.09	-0.01	#VALUE!

Table 16: MYO1B KD gene expression data. Relative quantification according to non-transfected cell line.

	DU145	PC3	SERBOB	MDA-Pca-2b
ACTB	0.00	0.00	0.00	0.00
CAV2	-0.15	0.05	0.04	#VALUE!
CD44	-0.21	0.04	-0.03	-0.35
CDH1	-0.18	0.10	-0.15	-0.08
CDH2	#VALUE!	0.07	-0.01	#VALUE!
CLDN3	-0.30	0.13	0.03	-0.11
COL11A1	#VALUE!	#VALUE!	#VALUE!	#VALUE!
CTNNB1	-0.16	0.11	0.03	-0.07
DPP4	0.01	0.13	0.01	-0.06
DSC1	#VALUE!	0.65	-0.06	1.25
EGFR	-0.07	-0.15	0.02	0.20
EPCAM	#VALUE!	#VALUE!	#VALUE!	#VALUE!
FN1	-0.22	0.14	0.06	-0.07
IGF1R	-0.44	0.11	-0.05	-0.14
ITGA4	#VALUE!	0.11	-0.18	#VALUE!
ITGA5	-0.14	0.28	0.02	0.19
ITGA8	#VALUE!	#VALUE!	#VALUE!	0.07
ITGAL	#VALUE!	#VALUE!	#VALUE!	#VALUE!
ITGAM	#VALUE!	#VALUE!	#VALUE!	#VALUE!
ITGAV	-0.08	0.10	0.01	-0.01
ITGB1	-0.18	0.18	-0.04	-0.08
ITGB2	-0.17	0.08	#VALUE!	-0.33
ITGB3	-0.30	#VALUE!	#VALUE!	#VALUE!
KRT19	-0.14	0.18	#VALUE!	-0.25
MET	-0.19	0.13	-0.02	0.18
PECAM1	#VALUE!	-0.21	#VALUE!	#VALUE!
PTK2	0.03	0.28	-0.08	-0.06
SNAI1	-0.06	0.19	-0.07	#VALUE!
SNAI2	-0.20	0.30	-0.07	#VALUE!
TWIST1	#VALUE!	-0.32	-0.05	-0.30
VASP	-0.25	0.25	-0.04	0.15
VIM	-0.10	0.12	-0.15	#VALUE!

Table 17: SPAG9 KD gene expression data. Relative quantification according to non-transfected cell line.

	DU145	PC3	SERBOB	MDA-Pca-2b
ACTB	0.00	0.00	0.00	0.00
CAV2	-0.10	0.10	-0.04	#VALUE!
CD44	-0.20	0.10	-0.06	-0.35
CDH1	-0.17	-0.10	-0.16	0.01
CDH2	#VALUE!	0.00	0.02	0.18
CLDN3	-0.18	0.06	0.14	-0.05
COL11A1	#VALUE!	#VALUE!	#VALUE!	#VALUE!
CTNNB1	-0.22	0.12	0.08	-0.01
DPP4	0.04	0.04	0.11	-0.11
DSC1	#VALUE!	0.16	0.23	0.89
EGFR	0.06	-0.14	-0.27	0.18
EPCAM	#VALUE!	#VALUE!	#VALUE!	#VALUE!
FN1	-0.12	0.17	0.08	0.07
IGF1R	-0.22	0.09	-0.07	-0.06
ITGA4	#VALUE!	0.19	0.19	#VALUE!
ITGA5	-0.14	0.27	0.22	0.14
ITGA8	#VALUE!	#VALUE!	#VALUE!	0.05
ITGAL	#VALUE!	#VALUE!	#VALUE!	#VALUE!
ITGAM	0.19	#VALUE!	#VALUE!	#VALUE!
ITGAV	-0.02	0.13	0.03	0.00
ITGB1	-0.15	0.16	0.03	0.03
ITGB2	-0.16	0.12	#VALUE!	-0.34
ITGB3	-0.21	#VALUE!	#VALUE!	#VALUE!
KRT19	-0.19	0.15	#VALUE!	-0.22
MET	-0.21	0.13	0.07	0.25
PECAM1	#VALUE!	-0.03	#VALUE!	#VALUE!
PTK2	-0.02	0.23	-0.03	0.01
SNAI1	-0.19	0.16	#VALUE!	#VALUE!
SNAI2	-0.26	0.35	-0.01	#VALUE!
TWIST1	#VALUE!	-0.25	-0.15	0.02
VASP	-0.25	0.29	0.01	0.31
VIM	-0.12	0.13	0.11	#VALUE!

Table 18: PRDM4 KD gene expression data. Relative quantification according to non-transfected cell line.

	DU145	PC3	MDA-Pca-2b
ACTB	0.00	0.00	0.00
CAV2	-0.28	0.01	#VALUE!
CD44	-0.26	0.04	-0.20
CDH1	-0.31	0.02	0.05
CDH2	#VALUE!	-0.09	0.15
CLDN3	-0.01	0.20	-0.02
COL11A1	#VALUE!	#VALUE!	#VALUE!
CTNNB1	-0.15	-0.10	0.06
DPP4	0.00	0.15	0.06
DSC1	#VALUE!	-0.16	1.55
EGFR	0.16	-0.02	0.18
EPCAM	#VALUE!	#VALUE!	#VALUE!
FN1	-0.24	0.04	0.06
IGF1R	-0.27	0.02	-0.28
ITGA4	#VALUE!	0.06	#VALUE!
ITGA5	-0.05	0.20	0.23
ITGA8	#VALUE!	#VALUE!	#VALUE!
ITGAL	#VALUE!	#VALUE!	#VALUE!
ITGAM	#VALUE!	#VALUE!	#VALUE!
ITGAV	0.02	0.11	0.19
ITGB1	-0.26	0.11	-0.09
ITGB2	-0.08	0.34	#VALUE!
ITGB3	#VALUE!	#VALUE!	#VALUE!
KRT19	-1.07	0.09	-0.16
MET	-0.34	0.03	#VALUE!
PECAM1	#VALUE!	0.10	#VALUE!
PTK2	-0.05	0.21	0.17
SNAI1	-0.15	0.16	#VALUE!
SNAI2	-0.90	0.21	#VALUE!
TWIST1	#VALUE!	-0.33	-0.21
VASP	-0.08	0.12	0.52
VIM	-0.10	-0.10	#VALUE!

Stable Knockdown Experiments

Table 19: DU145 cell line stable KD. Relative quantification according to non-transfected cell line.

	MYADM KD	MYO1B KD	PIP5K1A KD
ACTB	0.00	0.00	0.00
CAV2	-0.10	-0.01	0.04
CD44	0.51	0.63	0.67
CDH1	#DIV/0!	0.02	0.12
CDH2	#DIV/0!	#DIV/0!	#DIV/0!
CLDN3	0.02	-0.05	0.09
COL11A1	#DIV/0!	#DIV/0!	#DIV/0!
CTNNB1	0.37	0.38	0.54
DPP4	#DIV/0!	#DIV/0!	#DIV/0!
DSC1	#DIV/0!	0.04	0.07
EGFR	0.07	0.09	0.13
EPCAM	0.03	0.26	0.25
FN1	0.71	0.68	0.68
IGF1R	#DIV/0!	-0.21	-0.09
ITGA4	#DIV/0!	#DIV/0!	#DIV/0!
ITGA5	0.62	0.43	0.42
ITGA8	#DIV/0!	#DIV/0!	#DIV/0!
ITGAL	#DIV/0!	#DIV/0!	#DIV/0!
ITGAM	#DIV/0!	#DIV/0!	#DIV/0!
ITGAV	0.12	-0.01	0.07
ITGB1	-0.29	-0.10	-0.11
ITGB2	-0.36	-0.28	-0.18
ITGB3	#DIV/0!	#DIV/0!	#DIV/0!
KRT19	0.00	0.21	0.21
MET	0.37	0.50	0.41
PECAM1	1.12	0.54	0.61
PTK2	-0.17	-0.01	0.16
SNAI1	0.87	0.32	0.53
SNAI2	0.84	0.90	0.97
TWIST1	#DIV/0!	#DIV/0!	#DIV/0!
VASP	0.33	0.14	0.30
VIM	0.28	0.31	0.33

Table 20: PC3 cell line stable KD. Relative quantification according to non-transfected cell line.

	MYADM KD	MYO1B KD
ACTB	0.00	0.00
CAV2	-0.03	-0.18
CD44	-0.18	-0.21
CDH1	#DIV/0!	#DIV/0!
CDH2	0.39	0.49
CLDN3	0.31	0.28
COL11A1	#DIV/0!	#DIV/0!
CTNNB1	0.44	0.31
DPP4	#DIV/0!	#DIV/0!
DSC1	1.21	1.01
EGFR	-0.01	-0.14
EPCAM	-0.02	-0.07
FN1	0.17	-0.02
IGF1R	-0.59	-0.57
ITGA4	#DIV/0!	#DIV/0!
ITGA5	0.15	-0.14
ITGA8	#DIV/0!	#DIV/0!
ITGAL	0.55	#DIV/0!
ITGAM	#DIV/0!	#DIV/0!
ITGAV	0.13	0.11
ITGB1	-0.08	-0.12
ITGB2	0.03	0.07
ITGB3	#DIV/0!	#DIV/0!
KRT19	-0.25	-0.20
MET	0.16	0.13
PECAM1	0.76	0.62
PTK2	0.04	0.03
SNAI1	#DIV/0!	#DIV/0!
SNAI2	0.01	-0.17
TWIST1	-0.03	-0.08
VASP	-0.01	-0.05
VIM	0.11	0.10

Table 21: LNCaP cell line stable KD. Relative quantification according to non-transfected cell line.

	MYADM KD
ACTB	0.00
CAV2	0.33
CD44	0.19
CDH1	#DIV/0!
CDH2	#DIV/0!
CLDN3	#DIV/0!
COL11A1	#DIV/0!
CTNNB1	#DIV/0!
DPP4	#DIV/0!
DSC1	0.92
EGFR	#DIV/0!
EPCAM	-0.03
FN1	-0.66
IGF1R	#DIV/0!
ITGA4	#DIV/0!
ITGA5	-0.41
ITGA8	#DIV/0!
ITGAL	#DIV/0!
ITGAM	#DIV/0!
ITGAV	-0.69
ITGB1	-0.16
ITGB2	#DIV/0!
ITGB3	#DIV/0!
KRT19	#DIV/0!
MET	#DIV/0!
PECAM1	-0.14
PTK2	#DIV/0!
SNAI1	#DIV/0!
SNAI2	#DIV/0!
TWIST1	#DIV/0!
VASP	#DIV/0!
VIM	#DIV/0!

Table 22: VCaP cell line stable KD. Relative quantification according to non-transfected cell line.

	MYADM KD	MYO1B KD	PIP5K1A KD
ACTB	0.00	0.00	0.00
CAV2	#DIV/0!	#DIV/0!	#DIV/0!
CD44	0.42	0.36	0.28
CDH1	#DIV/0!	#DIV/0!	#DIV/0!
CDH2	#DIV/0!	#DIV/0!	#DIV/0!
CLDN3	-0.36	-0.12	-0.54
COL11A1	#DIV/0!	#DIV/0!	#DIV/0!
CTNNB1	0.12	0.03	#DIV/0!
DPP4	#DIV/0!	#DIV/0!	#DIV/0!
DSC1	0.56	0.51	0.63
EGFR	#DIV/0!	#DIV/0!	#DIV/0!
EPCAM	-0.12	-0.48	-0.81
FN1	-0.35	0.53	-0.24
IGF1R	#DIV/0!	#DIV/0!	#DIV/0!
ITGA4	#DIV/0!	#DIV/0!	#DIV/0!
ITGA5	#DIV/0!	#DIV/0!	#DIV/0!
ITGA8	#DIV/0!	#DIV/0!	#DIV/0!
ITGAL	#DIV/0!	#DIV/0!	#DIV/0!
ITGAM	#DIV/0!	#DIV/0!	#DIV/0!
ITGAV	-0.20	-0.25	0.11
ITGB1	-0.19	-0.48	-0.75
ITGB2	#DIV/0!	#DIV/0!	#DIV/0!
ITGB3	#DIV/0!	#DIV/0!	#DIV/0!
KRT19	-0.01	-0.05	#DIV/0!
MET	#DIV/0!	-0.49	#DIV/0!
PECAM1	#DIV/0!	#DIV/0!	#DIV/0!
PTK2	#DIV/0!	#DIV/0!	#DIV/0!
SNAI1	#DIV/0!	#DIV/0!	#DIV/0!
SNAI2	#DIV/0!	#DIV/0!	#DIV/0!
TWIST1	#DIV/0!	#DIV/0!	#DIV/0!
VASP	#DIV/0!	#DIV/0!	#DIV/0!
VIM	#DIV/0!	#DIV/0!	#DIV/0!

Pathways

The figures below (**Fig. 29–33**) illustrate the networks involving the detected biomarkers. Green indicates the desired biomarkers, while red indicates the genes that were further tested and are associated with the desirable biomarkers.

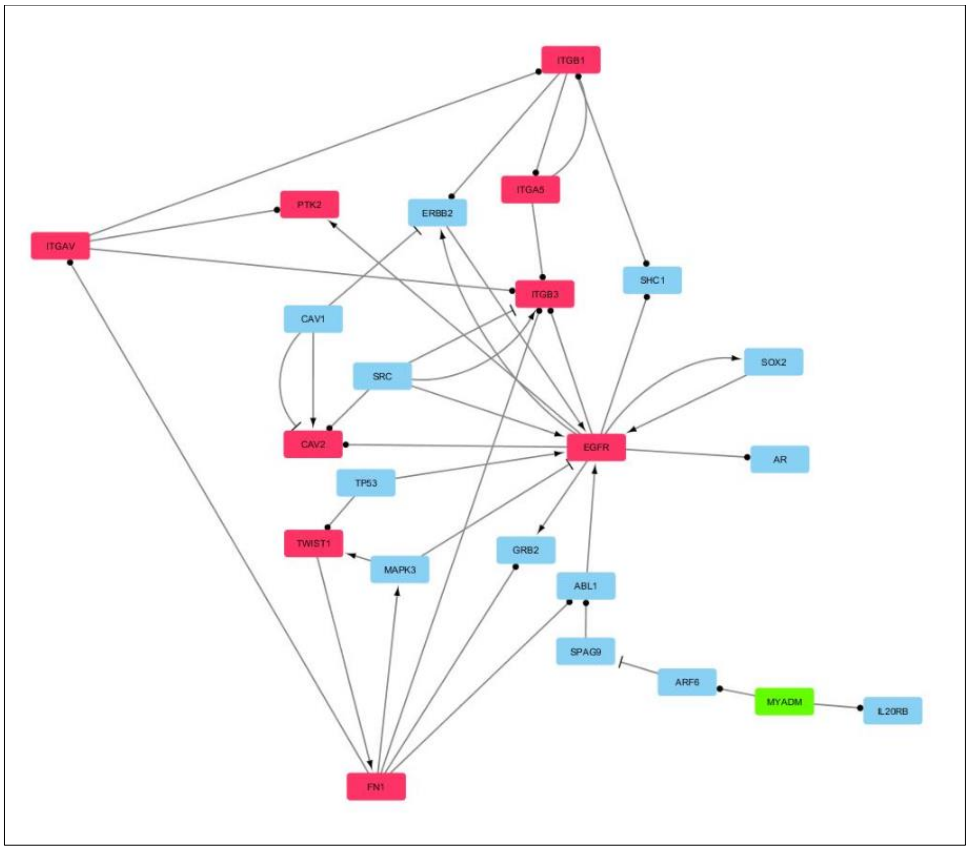

Figure 29: MYADM signaling transduction pathway.

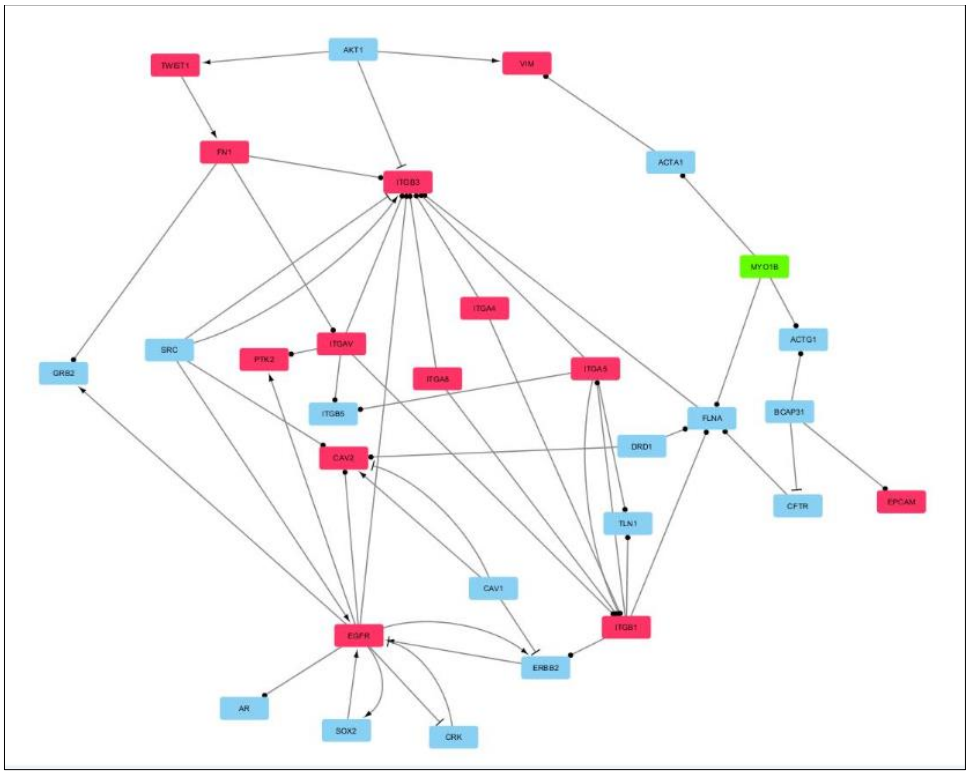

Figure 30: MYO1B signaling transduction pathway.

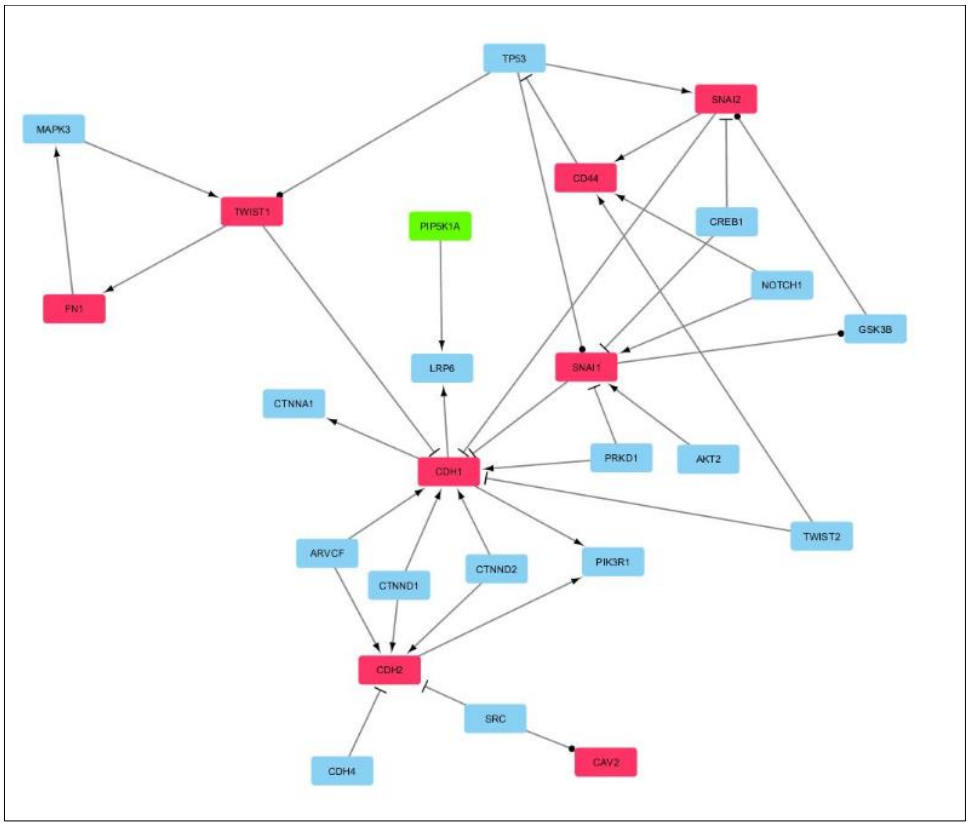

Figure 31: PIP5K1A signaling transduction pathway.

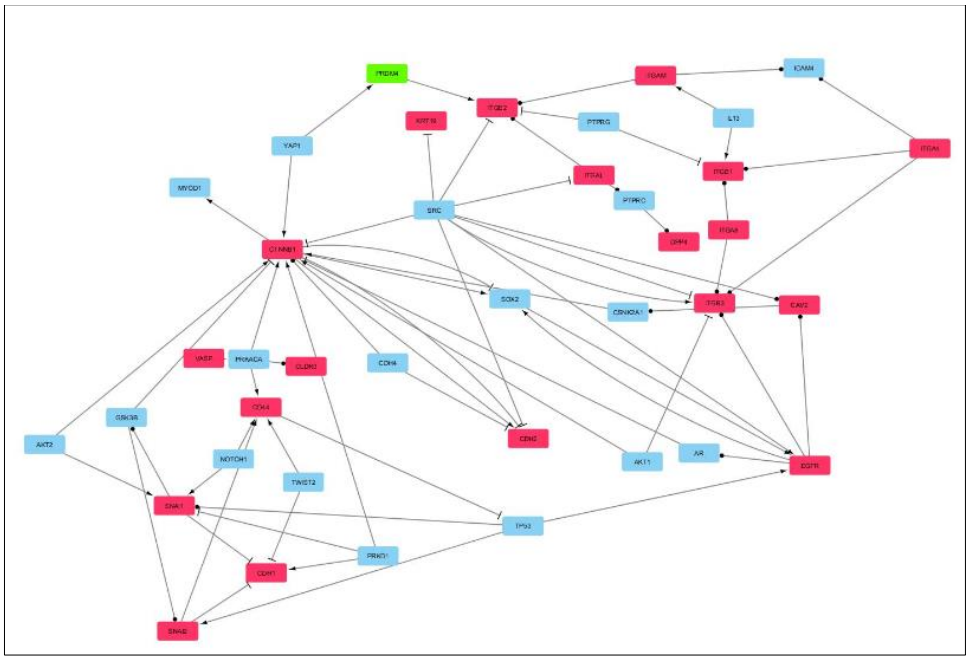

Figure 32: PRDM4 signaling transduction pathway.

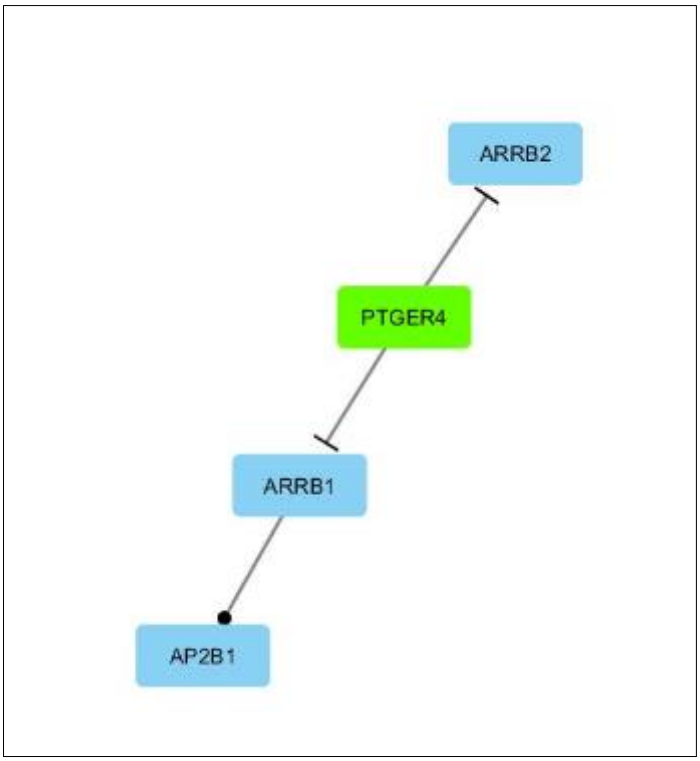

Figure 33: PTGER4 signaling transduction pathway.

→ : Activation

⊣ : Suppression

—● : Unknown function

Bibliography

Almeida, C. G., Yamada, A., Tenza, D., Louvard, D., Raposo, G., Coudrier, E. (2011): Myosin 1b promotes the formation of post-Golgi carriers by regulating actin assembly and membrane remodelling at the trans-Golgi network. Nat Cell Biol, 13(7), 779–789.

Aranda, J. F., Reglero-Real, N., Kremer, L., Marcos-Ramiro, B., Ruiz-Saenz, A., Calvo, M., Enrich, C., Correas, I., Millan, J., Alonso, M. A. (2011): MYADM regulates Rac1 targeting to ordered membranes required for cell spreading and migration. Mol Biol Cell, 22(8), 1252–1262.

Aranda, J. F., Reglero-Real, N., Marcos-Ramiro, B., Ruiz-Saenz, A., Fernandez-Martin, L., Bernabe-Rubio, M., Kremer, L., Ridley, A. J., Correas, I., Alonso, M. A., Millan, J. (2013): MYADM controls endothelial barrier function through ERM-dependent regulation of ICAM-1 expression. Mol Biol Cell, 24(4), 483–494.

Armstrong, R. A. (2014). When to use the Bonferroni correction. Ophthalmic & Physiological Optics, 34(5), 502–508. https://doi.org/10.1111/opo.12131

Attard, G., Rizzo, S., Ledaki, I., Clark, J., Reid, A. H., Thompson, A., Khoo, V., de Bono, J. S., Cooper, C. S., Hudson, D. L. (2009): A novel, spontaneously immortalized, human prostate cancer cell line, Bob, offers a unique model for pre-clinical prostate cancer studies. Prostate, 69(14), 1507–1520.

Autio, K. A., Morris, M. J. (2013): Targeting bone physiology for the treatment of metastatic prostate cancer. Clin Adv Hematol Oncol, 11(3), 134–143.

Baicu, S. C., Taylor, M. J. (2002): Acid-base buffering in organ preservation solutions as a function of temperature: New parameters for comparing buffer capacity and efficiency. Cryobiology, 45(1), 33–48. https://doi.org/10.1016/S0011-2240(02)00104-9

Cano, A., Perez-Moreno, M. A., Rodrigo, I., Locascio, A., Blanco, M. J., del Barrio, M. G., Portillo, F., Nieto, M. A. (2000): The transcription factor snail controls epithelial-mesenchymal transitions by repressing E-cadherin expression. Nat Cell Biol, 2(2), 76–83.

Chao, W. T., Daquinag, A. C., Ashcroft, F., Kunz, J. (2010): Type I PIPK-alpha regulates directed cell migration by modulating Rac1 plasma membrane targeting and activation. J Cell Biol, 190(2), 247–262.

Clark, P. R., Manes, T. D., Pober, J. S., Kluger, M. S. (2007): Increased ICAM-1 expression causes endothelial cell leakiness, cytoskeletal reorganization and junctional alterations. J Invest Dermatol, 127(4), 762–774.

D'Amico, A. V., Whittington, R., Kaplan, I., Beard, C., Schultz, D., Malkowicz, S. B., Wein, A., Tomaszewski, J. E., Coleman, C. N. (1998): Calculated prostate carcinoma volume: The optimal predictor of 3-year prostate specific antigen (PSA) failure free survival after surgery or radiation therapy of patients with pretreatment PSA levels of 4–20 nanograms per milliliter. Cancer, 82(2), 334–341.

Datta, K., Muders, M., Zhang, H., Tindall, D. J. (2010): Mechanism of lymph node metastasis in prostate cancer. Future Oncol, 6(5), 823–836.

Day, K. C., Lorenzatti Hiles, G., Kozminsky, M., Dawsey, S. J., Paul, A., Broses, L. J., Shah, R., Kunja, L. P., Hall, C., Palanisamy, N., Daignault-Newton, S., El-Sawy, L., Wilson, S. J., Chou, A., Ignatoski, K. W., Keller, E., Thomas, D., Nagrath, S., Morgan, T., Day, M. L. (2017): HER2 and EGFR Overexpression Support Metastatic Progression of Prostate Cancer to Bone. Cancer Res, 77(1), 74–85.

De Marzo, A. M., Bradshaw, C., Sauvageot, J., Epstein, J. I., Miller, G. J. (1998): CD44 and CD44v6 downregulation in clinical prostatic carcinoma: relation to Gleason grade and cytoarchitecture. Prostate, 34(3), 162–168.

Deep, G., Jain, A. K., Ramteke, A., Ting, H., Vijendra, K. C., Gangar, S. C., Agarwal, C., Agarwal, R. (2014): SNAI1 is critical for the aggressiveness of prostate cancer cells with low E-cadherin. Mol Cancer, 13, 37.

Diz-Muñoz, A., Krieg, M., Bergert, M., Ibarlucea-Benitez, I., Muller, D. J., Paluch, E., Heisenberg, C. P. (2010): Control of directed cell migration in vivo by membrane-to-cortex attachment. PLoS Biol, 8(11), e1000544.

Edmondson, R., Adcock, A. F., Yang, L. (2016): Influence of Matrices on 3D-Cultured Prostate Cancer Cells' Drug Response and Expression of Drug-Action Associated Proteins. PLoS One, 11(6), e0158116.

Ekinci, F., Yildizdas, R. D., Horoz, O. O., Herguner, O., Bisgin, A. (2020). A homozygote frameshift mutation in OCLN gene result in Pseudo-TORCH syndrome type I: A case report extending the phenotype with central diabetes insipidus and renal dysfunction. European Journal of Medical Genetics, 63(6). https://doi.org/10.1016/j.ejmg.2020.103923

Emadi Baygi, M., Soheili, Z. S., Essmann, F., Deezagi, A., Engers, R., Goering, W., Schulz, W. A. (2010): Slug/SNAI2 regulates cell proliferation and invasiveness of metastatic prostate cancer cell lines. Tumour Biol, 31(4), 297–307.

Fehon, R. G., McClatchey, A. I., Bretscher, A. (2010): Organizing the cell cortex: the role of ERM proteins. Nat Rev Mol Cell Biol, 11(4), 276–287.

Flemming, A. (2014): Cancer: Lipid kinase PIP5K1alpha as a new target in prostate cancer. Nat Rev Drug Discov, 13(10), 723.

Francis, J. C., Thomsen, M. K., Taketo, M. M., Swain, A. (2013): Beta-catenin is required for prostate development and cooperates with Pten loss to drive invasive carcinoma. PLoS Genet, 9(1), e1003180.

Furuse, M., Hirase, T., Itoh, M., Nagafuchi, A., Yonemura, S., Tsukita, S., Tsukita, S. (1993): Occludin: A novel integral membrane protein localizing at tight junctions. J Cell Biol, 123(6), 1777–1788. https://doi.org/10.1083/jcb.123.6.1777

Gabriele, D., Jereczek-Fossa, B. A., Krengli, M., Garibaldi, E., Tessa, M., Moro, G., Girelli, G., Gabriele, P. (2016): Beyond D'Amico risk classes for predicting recurrence after external beam radiotherapy for prostate cancer: the Candiolo classifier. Radiat Oncol, 11, 23.

Gajula, R. P., Chettiar, S. T., Williams, R. D., Thiyagarajan, S., Kato, Y., Aziz, K., Wang, R., Gandhi, N., Wild, A. T., Vesuna, F., Ma, J., Salih, T., Cades, J., Fertig, E., Biswal, S., Burns, T. F., Chung, C. H., Rudin, C. M., Herman, J. M., Hales, R. K., Raman, V., An, S. S., Tran, P. T. (2013): The twist box domain is required for Twist1-induced prostate cancer metastasis. Mol Cancer Res, 11(11), 1387–1400.

Hammer, Ø., Harper, D. A. T., Ryan, P. D. (2001): PAST: Paleontological statistics software package for education and data analysis. Palaeontologia Electronica. https://palaeo-electronica.org/2001_1/past/past.pdf

He, M., He, Q., Cai, X., Chen, Z., Lao, S., Deng, H., … He, J. (2021): Role of lymphatic endothelial cells in the tumor microenvironment—a narrative review of recent advances. Translational Lung Cancer Research, 10(5). https://doi.org/10.21037/tlcr-21-40

Heidegger, I., Kern, J., Ofer, P., Klocker, H., Massoner, P. (2014): Oncogenic functions of IGF1R and INSR in prostate cancer include enhanced tumor growth, cell migration and angiogenesis. Oncotarget, 5(9), 2723–2735.

Heissler, S. M., Sellers, J. R. (2016): Kinetic Adaptations of Myosins for Their Diverse Cellular Functions. Traffic, 17(8), 839–859.

Horoszewicz, J. S., Leong, S. S., Kawinski, E., Karr, J. P., Rosenthal, H., Chu, T. M., Mirand, E. A., Murphy, G. P. (1983): LNCaP model of human prostatic carcinoma. Cancer Res, 43(4), 1809–1818.

Huang, T., Wang, L., Liu, D., Li, P., Xiong, H., Zhuang, L., Sun, L., Yuan, X., Qiu, H. (2017): FGF7/FGFR2 signal promotes invasion and migration in human gastric cancer through upregulation of thrombospondin-1. Int J Oncol, 50(5), 1501–1512.

Jędroszka, D., Orzechowska, M., Hamouz, R., Górniak, K., Bednarek, A. K. (2017): Markers of epithelial-to-mesenchymal transition reflect tumor biology according to patient age and Gleason score in prostate cancer. PLoS ONE. https://doi.org/10.1371/journal.pone.0188842

Jiang, L., Yang, Y. D., Fu, L., Xu, W., Liu, D., Liang, Q., Zhang, X., Xu, L., Guan, X. Y., Wu, B., Sung, J. J., Yu, J. (2014): CLDN3 inhibits cancer aggressiveness via Wnt-EMT signaling and is a potential prognostic biomarker for hepatocellular carcinoma. Oncotarget, 5(17), 7663–7676.

Jiang, Y., Dai, J., Yao, Z., Shelley, G., Keller, E. T. (2017): Abituzumab Targeting of alphaV-Class Integrins Inhibits Prostate Cancer Progression. Mol Cancer Res, 15(7), 875–883.

Kamibeppu, T., Yamasaki, K., Nakahara, K., Nagai, T., Terada, N., Tsukino, H., Mukai, S., Kamoto, T. (2018): Caveolin-1 and -2 regulate cell motility in castration-resistant prostate cancer. Res Rep Urol, 10, 135–144.

Keil, K. P., Abler, L. L., Mehta, V., Altmann, H. M., Laporta, J., Plisch, E. H., Suresh, M., Hernandez, L. L., Vezina, C. M. (2014): DNA methylation of E-cadherin is a priming mechanism for prostate development. Dev Biol, 387(2), 142–153.

Komaba, S., Coluccio, L. M. (2010): Localization of myosin 1b to actin protrusions requires phosphoinositide binding. J Biol Chem, 285(36), 27686–27693.

Korenchuk, S., Lehr, J. E., McLean, L., Lee, Y. G., Whitney, S., Vessella, R., Lin, D. L., Pienta, K. J. (2001): VCaP, a cell-based model system of human prostate cancer. In Vivo, 15(2), 163–168.

Kwiatkowska, K. (2010): One lipid, multiple functions: how various pools of PI(4,5)P(2) are created in the plasma membrane. Cell Mol Life Sci, 67(23), 3927–3946.

Laidler, P., Dulinska, J., Lekka, M., Lekki, J. (2005): Expression of prostate specific membrane antigen in androgen-independent prostate cancer cell line PC-3. Arch Biochem Biophys, 435(1), 1–14.

Lee, J. M., Dedhar, S., Kalluri, R., Thompson, E. W. (2006): The epithelial-mesenchymal transition: new insights in signaling, development, and disease. J Cell Biol, 172(7), 973–981. https://doi.org/jcb.200601018 [pii]10.1083/jcb.200601018

Li, H., Peng, Y., Niu, H., Wu, B., Zhang, Y., Bai, X., He, P. (2014): SPAG9 is overexpressed in human prostate cancer and promotes cancer cell proliferation. Tumour Biol, 35(7), 6949–6954.

Liu, F., Shangli, Z., Hu, Z. (2018): CAV2 promotes the growth of renal cell carcinoma through the EGFR/PI3K/Akt pathway. Onco Targets Ther, 11, 6209-6216.

Liu, H., Dai, X., Cao, X., Yan, H., Ji, X., Zhang, H., Shen, S., Si, Y., Chen, J., Li, L., Zhao, J. C., Yu, J., Feng, X. H., Zhao, B. (2018): PRDM4 mediates YAP-induced cell invasion by activating leukocyte-specific integrin beta2 expression. EMBO Rep, 19(6).

Liu, P., Liang, Y., Jiang, L., Wang, H., Wang, S., Dong, J. (2018): CX3CL1/fractalkine enhances prostate cancer spinal metastasis by activating the Src/FAK pathway. Int J Oncol, 53(4), 1544-1556.

Livak, K. J., Schmittgen, T. D. (2001): Analysis of relative gene expression data using real-time quantitative PCR and the 2(-Delta Delta C(T)) Method. Methods, 25(4), 402–408.

Makowska, K. A., Hughes, R. E., White, K. J., Wells, C. M., Peckham, M. (2015): Specific Myosins Control Actin Organization, Cell Morphology, and Migration in Prostate Cancer Cells. Cell Rep, 13(10), 2118–2125.

Mellman, D. L., Gonzales, M. L., Song, C., Barlow, C. A., Wang, P., Kendziorski, C., Anderson, R. A. (2008): A PtdIns4,5P2-regulated nuclear poly(A) polymerase controls expression of select mRNAs. Nature, 451(7181), 1013-7.

Morin, P. J. (2005): Claudin proteins in human cancer: promising new targets for diagnosis and therapy. Cancer Res, 65(21), 9603–9606.

MTSU (Middle Tennessee State University) (n. d.): Determination of calcium by Standardized EDTA Solution. https://www.mtsu.edu/chemistry/chem2230/pdfs/Exp9A.pdf

Mustafa, M., Salih, A. F., Illzam, E. M., Sharifa, A. M., Suleiman, M., Hussain, S. S. (2016): Prostate Cancer: Pathophysiology, Diagnosis, and Prognosis. J Med Dent Sci, 15(6), 4–11.

Myklebust, M. P., Fluge, O., Immervoll, H., Skarstein, A., Balteskard, L., Bruland, O., Dahl, O. (2012): Expression of DSG1 and DSC1 are prognostic markers in anal carcinoma patients. Br J Cancer, 106(4), 756–762.

Navone, N. M., Olive, M., Ozen, M., Davis, R., Troncoso, P., Tu, S. M., Johnston, D., Pollack, A., Pathak, S., von Eschenbach, A. C., Logothetis, C. J. (1997): Establishment of two human prostate cancer cell lines derived from a single bone metastasis. Clin Cancer Res, 3(12 Pt 1), 2493–2500.

Niu, J., Chang, Z., Peng, B., Xia, Q., Lu, W., Huang, P., Tsao, M. S., Chiao, P. J. (2007): Keratinocyte growth factor/fibroblast growth factor-7-regulated cell migration and invasion through activation of NF-kappaB transcription factors. J Biol Chem, 282(9), 6001–6011.

Ohmura, G., Tsujikawa, T., Yaguchi, T., Kawamura, N., Mikami, S., Sugiyama, J., Nakamura, K., Kobayashi, A., Iwata, T., Nakano, H., Shimada, T., Hisa, Y., Kawakami, Y. (2015):

Aberrant Myosin 1b Expression Promotes Cell Migration and Lymph Node Metastasis of HNSCC. Mol Cancer Res, 13(4), 721–731.

Omara-Opyene, A. L., Qiu, J., Shah, G. V., Iczkowski, K. A. (2004): Prostate cancer invasion is influenced more by expression of a CD44 isoform including variant 9 than by Muc18. Lab Invest, 84(7), 894–907.

Peinado, H., Olmeda, D., Cano, A. (2007): Snail, Zeb and bHLH factors in tumour progression: an alliance against the epithelial phenotype?. Nat Rev Cancer, 7(6), 415–428.

Pellinen, T., Blom, S., Sanchez, S., Valimaki, K., Mpindi, J. P., Azegrouz, H., Strippoli, R., Nieto, R., Viton, M., Palacios, I., Turkki, R., Wang, Y., Sanchez-Alvarez, M., Nordling, S., Butzow, A., Mirtti, T., Rannikko, A., Montoya, M. C., Kallioniemi, O., Del Pozo, M. A. (2018): ITGB1-dependent upregulation of Caveolin-1 switches TGFbeta signalling from tumour-suppressive to oncogenic in prostate cancer. Sci Rep, 8(1), 2338.

Preisser, F., van den Bergh, R. C. N., Gandaglia, G., Ost, P., Surcel, C. I., Sooriakumaran, P., Montorsi, F., Graefen, M., van der Poel, H., de la Taille, A., Briganti, A., Salomon, L., Ploussard, G., Tilki, D. (2020): Effect of Extended Pelvic Lymph Node Dissection on Oncologic Outcomes in Patients with D'Amico Intermediate and High Risk Prostate Cancer Treated with Radical Prostatectomy: A Multi-Institutional Study. J Urol, 203(2), 338–343.

Ravipaty, S., Wu, W., Dalvi, A., Tanna, N., Andreazi, J., Friss, T., Klotz, A., Liao, C., Garren, J., Schofield, S., Diamandis, E. P., Klein, E. A., Dobi, A., Srivastava, S., Tekumalla, P., Kiebish, M. A., Vishnudas, V., Sarangarajan, R. P., Narain, N. R., Akmaev, V. R. (2017): Clinical Validation of a Serum Protein Panel (FLNA, FLNB and KRT19) for Diagnosis of Prostate Cancer. J Mol Biomark Diagn, 8(2), 323.

Reynolds, A., Leake, D., Boese, Q., Scaringe, S., Marshall, W. S., Khvorova, A. (2004): Rational siRNA design for RNA interference. Nat Biotechnol, 22(3), 326–330.

Ridley, A. J., Schwartz, M. A., Burridge, K., Firtel, R. A., Ginsberg, M. H., Borisy, G., Parsons, J. T., Horwitz, A. R. (2003): Cell migration: integrating signals from front to back. Science, 302(5651), 1704–1709.

Russo, J. W., Gao, C., Bhasin, S. S., Voznesensky, O. S., Calagua, C., Arai, S., Nelson, P. S., Montgomery, B., Mostaghel, E. A., Corey, E., Taplin, M. E., Ye, H., Bhasin, M., Balk, S. P. (2018): Downregulation of Dipeptidyl Peptidase 4 Accelerates Progression to Castration-Resistant Prostate Cancer. Cancer Res, 78(22), 6354–6362. https://doi.org/10.1158/0008-5472.CAN-18-0687

Schober, P., Vetter, T. R. (2020). Analysis of Variance in Medical Research. Anesthesia and Analgesia, 131(2), 508–509. https://doi.org/10.1213/ANE.0000000000004839

Semenas, J., Hedblom, A., Miftakhova, R. R., Sarwar, M., Larsson, R., Shcherbina, L., Johansson, M. E., Harkonen, P., Sterner, O., Persson, J. L. (2014): The role of PI3K/AKT-related PIP5K1alpha and the discovery of its selective inhibitor for treatment of advanced prostate cancer. Proc Natl Acad Sci U S A, 111(35), E3689–3698.

Smith, H. A., McNeel, D. G. (2010): The SSX family of cancer-testis antigens as target proteins for tumor therapy. Clin Dev Immunol, 2010, 150591.

Stone, K. R., Mickey, D. D., Wunderli, H., Mickey, G. H., Paulson, D. F. (1978): Isolation of a human prostate carcinoma cell line (DU 145). Int J Cancer, 21(3), 274–281.

Sun, H. F., Wang, W. D., Feng, L. (2017): Effect of SPAG9 on migration, invasion and prognosis of prostate cancer. Int J Clin Exp Pathol, 10(9), 9468–9474.

van der Horst, G., van den Hoogen, C., Buijs, J. T., Cheung, H., Bloys, H., Pelger, R. C., Lorenzon, G., Heckmann, B., Feyen, J., Pujuguet, P., Blanque, R., Clement-Lacroix, P., van der Pluijm, G. (2011): Targeting of alpha(v)-integrins in stem/progenitor cells and supportive microenvironment impairs bone metastasis in human prostate cancer. Neoplasia, 13(6), 516–525.

Voeller, H. J., Truica, C. I., Gelmann, E. P. (1998): Beta-catenin mutations in human prostate cancer. Cancer Res, 58(12), 2520–2523.

Ware, J. L., Paulson, D. F., Mickey, G. H., Webb, K. S. (1982): Spontaneous metastasis of cells of the human prostate carcinoma cell line PC-3 in athymic nude mice. J Urol, 128(5), 1064–1067.

Watanabe, K., Tominari, T., Hirata, M., Matsumoto, C., Maruyama, T., Murphy, G., Nagase, H., Miyaura, C., Inada, M. (2016): Abrogation of prostaglandin E-EP4 signaling in osteoblasts prevents the bone destruction induced by human prostate cancer metastases. Biochem Biophys Res Commun, 478(1), 154–161.

Wei, J., Xu, G., Wu, M., Zhang, Y., Li, Q., Liu, P., Zhu, T., Song, A., Zhao, L., Han, Z., Chen, G., Wang, S., Meng, L., Zhou, J., Lu, Y., Ma, D. (2008): Overexpression of vimentin contributes to prostate cancer invasion and metastasis via src regulation. Anticancer Res, 28(1A), 327–334.

Wheelock, M. J., Shintani, Y., Maeda, M., Fukumoto, Y., Johnson, K. R. (2008): Cadherin switching. J Cell Sci, 121(Pt 6), 727–735.

Yamada, A., Mamane, A., Lee-Tin-Wah, J., Di Cicco, A., Prevost, C., Levy, D., Joanny, J. F., Coudrier, E., Bassereau, P. (2014): Catch-bond behaviour facilitates membrane tubulation by non-processive myosin 1b. Nat Commun, 5, 3624.

Yousef, G. M., Scorilas, A., Magklara, A., Memari, N., Ponzone, R., Sismondi, P., Biglia, N., Abd Ellatif, M., Diamandis, E. P. (2002): The androgen-regulated gene human kallikrein 15 (KLK15) is an independent and favourable prognostic marker for breast cancer. Br J Cancer, 87(11), 1294–1300.

Yu, C., Gong, Y., Zhou, H., Wang, M., Kong, L., Liu, J., An, T., Zhu, H., Li, Y. (2017): Star-PAP, a poly(A) polymerase, functions as a tumor suppressor in an orthotopic human breast cancer model. Cell Death Dis, 8(2), e2582.

Zhang, H. R., Lai, S. Y., Huang, L. J., Zhang, Z. F., Liu, J., Zheng, S. R., Ding, K., Bai, X., Zhou, J. Y. (2018): Myosin 1b promotes cell proliferation, migration, and invasion in cervical cancer. Gynecol Oncol, 149(1), 188–197.

Zhao, Y., Yan, Q., Long, X., Chen, X., Wang, Y. (2008): Vimentin affects the mobility and invasiveness of prostate cancer cells. Cell Biochem Funct, 26(5), 571–577.

Acknowledgements

This work is dedicated to all mentors, teachers, and supporters who have shown me the way to discovery. Particularly, I would like to express my deepest gratitude to my supervising professor Dr. med. Klaus-Peter Jünemann who offered me the opportunity to conduct this research. Also, I would like to thank my family and my collaborators for their patience and support during the entire time of this research.